Eur. Phys. J. Plus (2025) 140:1184
https://doi.org/10.1140/epjp/s13360-025-07064-8

THE EUROPEAN PHYSICAL JOURNAL PLUS

Regular Article

Vacuum polarization current in presence of intense Sauter field

Deepak Sah[1,2,a], **Manoranjan P. Singh**[1,2]

[1] Theory and Simulations Lab, Theoretical and Computational Physics Section, Raja Ramanna Centre for Advanced Technology, Indore 452013, India
[2] Homi Bhabha National Institute, Training School Complex, Anushakti Nagar, Mumbai 400094, India

Received: 18 July 2025 / Accepted: 11 November 2025

Abstract The spontaneous creation of particle-antiparticle pairs from vacuum fluctuations under strong electromagnetic fields - known as the Sauter-Schwinger effect - represents one of quantum electrodynamics' most profound nonperturbative predictions. A well-known difficulty, however, is that the time-dependent particle number defined via Bogoliubov transformations lacks an unambiguous physical meaning during the field's evolution, becoming well-defined only once the external field is switched off. This raises the need for alternative observables that remain physically meaningful at all times. Here, we demonstrate that the vacuum polarization current provides such an observable. Focusing on scalar QED in $(1+1)$ dimensions with a time-dependent Sauter field, we compute the polarization current and analyze its relation to the particle correlation function. We find that the current, unlike the particle number, does not saturate at late times but instead exhibits persistent oscillations around zero–a distinctive signature of scalar systems. Remarkably, this current is shown to be largely unaffected by the choice of adiabatic basis, underscoring its robustness as a probe of pair-creation dynamics.

1 Introduction

The creation of particle-antiparticle pairs from the quantum vacuum under intense electromagnetic or gravitational fields is a cornerstone of quantum field theory (QFT). Pioneered by Klein [1, 2] and Sauter [3, 4] in the 1930 s using relativistic quantum mechanics, this phenomenon found its rigorous description only within QFT, where pair production arises from the interaction of quantum fields with time-dependent external potentials. Two prominent examples include cosmological particle production (driven by spacetime dynamics [5, 6]) and the Schwinger effect, where strong electric fields trigger vacuum decay [7–9]. As a key prediction of nonperturbative quantum electrodynamics (QED), the Schwinger effect remains experimentally elusive due to its exponential suppression for electric fields below the critical threshold $E_c = \frac{m^2}{e} \simeq 1.32 \times 10^{18}$ V/m, as first noted in [2]. However, next-generation laser facilities-such as ELI-NP [10–12], DESY's XFEL [13, 14], and CoReLS [15] are now poised to probe this regime, enabling tests of strong-field QED phenomena [16, 17]. These ultra-intense laser pulses have significantly impacted fields such as relativistic nonlinear optics, high-field QED, high-energy particle physics, and laboratory astrophysics [18, 19].

Beyond high-energy physics, vacuum pair production manifests in condensed matter systems, notably graphene [20–23]. Monolayer graphene's low-energy excitations under electromagnetic fields obey the (2+1)-dimensional Dirac equation [24–28], enabling analog studies of QED phenomena. Experiments have observed nonlinear current–voltage responses attributed to pair creation [29], spurring theoretical work on supercritical fields and production limits in these systems [20, 30–32].

Ultra-intense laser experiments now offer a pathway to test vacuum pair creation as a prototypical nonperturbative QFT effect [19, 33, 34], circumventing traditional perturbative methods. Theoretically, this phenomenon is intimately tied to quantum vacuum structure [35–37].

In the canonical quantization of matter fields, vacuum states are typically defined by preserving the symmetries of the classical theory. In Minkowski spacetime, Poincaré symmetry uniquely determines the annihilation and creation operators, yielding a well-defined vacuum. However, when a time-dependent external field is present, time translation symmetry is broken, rendering the particle concept ambiguous [38, 39]. Different vacuum state choices lead to distinct quantum theories, each with its own particle definition. Several vacuum selection criteria have been proposed, including adiabatic vacua [40], Hamiltonian diagonalization [41, 42], and minimization of the renormalized stress-energy tensor [43, 44].

An evolving external field dynamically modifies the system's vacuum state, resulting in particle-antiparticle pair creation. The time-dependent number of created pairs, $\mathcal{N}(t)$, depends on the chosen vacuum state for comparison [45]. While the particle concept becomes well-defined at asymptotic times after the external field vanishes [46, 47], particle definitions remain ambiguous during the

[a] e-mail: dsah129@gmail.com (corresponding author)

Published online: 10 December 2025

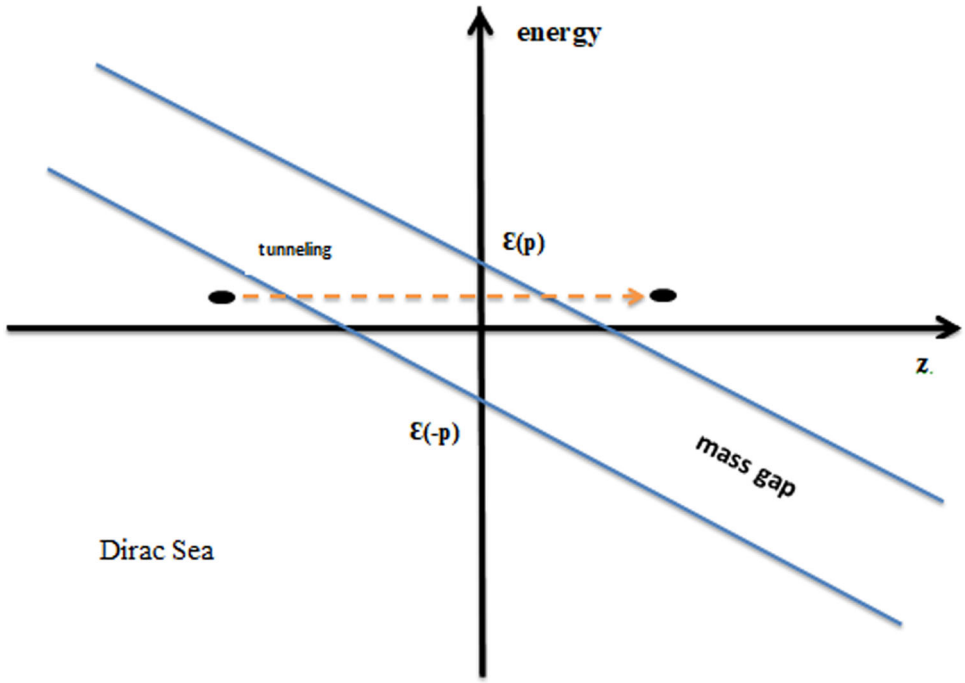

Fig. 1 Schematic illustration of the tunneling process in pair production

field's evolution. This necessitates alternative approaches like quasi-particle descriptions [48, 49], raising the fundamental question: Is there a well-defined observable that characterizes pair production dynamics at all times, not just asymptotically?

A promising candidate is the vacuum polarization current density, which maintains physical meaning throughout the entire time evolution. This can be understood through a classical analogy of electric dipole variation. Motivated by this, we analyze the behavior of the vacuum polarization current density. In the present work, we focus on the generic features of this observable to gain insights into the intermediate-time behavior of dynamical variables in the system's evolution equations.

The polarization current can be understood through the variation of an electric dipole within the canonical quantization framework. Consider a particle-antiparticle pair created with momenta $\boldsymbol{p}$ and $-\boldsymbol{p}$. When these particles become on-shell, their energy is $\varepsilon(\boldsymbol{p}) = \sqrt{\boldsymbol{p}^2 + m^2}$, and their separation is given by $2\frac{\varepsilon(\boldsymbol{p})}{eE}$, forming an electric dipole of magnitude $2\frac{\varepsilon(\boldsymbol{p})}{E}$, where the electric charge e (see Fig. 1). Since the polarization current originates from the time variation of these electric dipoles, its creation rate is determined by $\frac{d}{dt}\mathcal{N}(\boldsymbol{p}, t)$. Thus, the total dipole variation rate, corresponding to the polarization current, is $J_{\rm pol}(t) = \int [d\boldsymbol{p}]\, 2\frac{\varepsilon(\boldsymbol{p})}{E}\frac{d}{dt}\mathcal{N}(\boldsymbol{p}, t)$. In the quantum kinetic formalism, the particle creation rate connects to the single-particle state correlation function: $\frac{d}{dt}\mathcal{N}(\boldsymbol{p}, t) \propto \Re[\mathcal{C}(\boldsymbol{p}, t)]$, demonstrating its relation to the polarization current.

To analyze this effect quantitatively, we introduce the pair correlation function $\mathcal{C}(\boldsymbol{p}, t) = \langle 0|\hat{a}^\dagger(\boldsymbol{p}, t)\hat{b}^\dagger(-\boldsymbol{p}, t)|0\rangle$, which quantifies the amplitude for creating a particle-antiparticle pair with opposite momenta from the vacuum. Its real and imaginary parts, $u(\boldsymbol{p}, t) = \mathrm{Re}[\mathcal{C}(\boldsymbol{p}, t)]$ and $v(\boldsymbol{p}, t) = \mathrm{Im}[\mathcal{C}(\boldsymbol{p}, t)]$, have distinct physical roles. The function $u(\boldsymbol{p}, t)$ characterizes the instantaneous vacuum polarization, representing the coherent fluctuations of pairs aligned by the external field. Its counterpart, $v(\boldsymbol{p}, t)$, governs the depolarization dynamics, acting as a counter-term that restores the vacuum. As we will show, their coupled evolution captures the essential physics of pair creation and annihilation, and $u(\boldsymbol{p}, t)$ is directly linked to the polarization current density.

In this work, we study scalar QED in a spatially homogeneous, time-dependent electric field. Specifically, we consider a Sauter-type electric field profile, which permits analytical solutions for both the particle number distribution [50–54] and pair production dynamics [55, 56]. We first revisit the standard expression for the temporal evolution of particle number, incorporating arbitrary mode selections through Bogoliubov transformations in the canonical quantization approach. The particle number evolution displays distinct dynamical stages, analogous to those shown for spin-1/2 fermions in Ref. [57]. Natural choices of reference mode functions produce results equivalent to those from quantum kinetic formalism [58, 59].

We then derive generalized expressions for both the number of created particles and particle correlation functions, with particular focus on the evolution of $\mathcal{C}(\boldsymbol{p}, t)$, which to our knowledge has not been thoroughly investigated in this context. We compute the time-dependent particle correlation function for an intense Sauter field and analyze its dynamical characteristics, examining how the polarization functions $u(\boldsymbol{p}, t)$ and $v(\boldsymbol{p}, t)$ evolve under varying field parameters.

Finally, we demonstrate that the polarization current $J_{\rm pol}(t)$, derived from the gauge-invariant Noether current [30, 60] and proportional to $u(\boldsymbol{p}, t)$, provides a physical quantity that remains largely unaffected by the choice of adiabatic basis. This establishes the polarization current as a unique, well-defined probe of quantum vacuum dynamics at all times.

The paper is structured as follows. Section 2 presents a detailed theoretical formulation of the problem, building upon the derivations in Refs. [61, 62] while maintaining self-contained completeness. Section 3 introduces generalized expressions for both the number of created particles and particle correlation functions, incorporating arbitrary quantization mode choices through Bogoliubov transformations. In Sect. 4, we derive the time-dependent particle correlation function for an intense Sauter field, with Sect. 5 analyzing its dynamical characteristics. Section 6 examines the basis dependence of the polarization current. We conclude with a summary of key findings.

Throughout this work, we employ natural units with $\hbar = c = m = |e| = 1$, where the electron charge $e < 0$. All quantities are expressed in units of the electron mass.

2 Theory

Let us consider a charged scalar field $\Phi(t, \boldsymbol{x})$ of mass m and charge e in the presence of a spatially homogeneous, time-dependent classical electric field described by the four-vector potential A_μ. This setup is analogous to particle-creation scenarios induced by other time-dependent external agents or involving different matter fields (e.g., Dirac fields). Its dynamics is determined by the Klein-Gordon equation

$$\left[(\partial^\mu + ieA^\mu)(\partial_\mu + ieA_\mu) + m^2\right]\Phi(t, \boldsymbol{x}) = 0, \tag{1}$$

where A_μ is the external electromagnetic potential. We work in the temporal gauge $A_\mu = (0, A(t))$, which preserves the spatial homogeneity of the electric field $E(t) = -\dot{A}(t)$. Throughout this work, we neglect backreaction effects of the quantum test fields.

After Fourier transformation,

$$\phi(\boldsymbol{p}, t) = \int \frac{d^3x}{(2\pi)^{3/2}} e^{-i\boldsymbol{p}\cdot\boldsymbol{x}} \Phi(t, \boldsymbol{x}), \tag{2}$$

the time-dependent momentum modes satisfy decoupled second order differential equations:

$$\ddot{\phi}(\boldsymbol{p}, t) + \omega^2(\boldsymbol{p}, t)\phi(\boldsymbol{p}, t) = 0, \tag{3}$$

with time-dependent frequencies

$$\omega(\boldsymbol{p}, t) = \sqrt{[\boldsymbol{p} + e\boldsymbol{A}(t)]^2 + m^2}. \tag{4}$$

The complex scalar modes $\phi(\boldsymbol{p}, t)$ can be decomposed into real and imaginary parts, each satisfying Eq. (3). Hence, without loss of generality, we may treat $\phi(\boldsymbol{p}, t)$ as real.

2.1 Canonical quantization

Let $f(\boldsymbol{p}, t)$ be a particular complex solution of Eq. (3). The general solution can then be written as

$$\begin{pmatrix} \phi(\boldsymbol{p}, t) \\ \pi(\boldsymbol{p}, t) \end{pmatrix} = \boldsymbol{M}_1 \begin{pmatrix} a(\boldsymbol{p}) \\ b^*(\boldsymbol{p}) \end{pmatrix} \tag{5}$$

$$\boldsymbol{M}_1 = \begin{pmatrix} f(\boldsymbol{p}, t) & f^*(\boldsymbol{p}, t) \\ \dot{f}(\boldsymbol{p}, t) & \dot{f}^*(\boldsymbol{p}, t) \end{pmatrix} \tag{6}$$

where $a(\boldsymbol{p})$ and $b^*(\boldsymbol{p})$ are the annihilation and creation variables.

More generally, the solutions $\phi(\boldsymbol{p}, t)$ and $\pi(\boldsymbol{p}, t)$ can be expressed in terms of arbitrary complex functions $\chi(\boldsymbol{p}, t)$ and $\psi(\boldsymbol{p}, t)$:

$$\begin{pmatrix} \phi(\boldsymbol{p}, t) \\ \pi(\boldsymbol{p}, t) \end{pmatrix} = \boldsymbol{M}_2 \begin{pmatrix} a(\boldsymbol{p}, t) \\ b^*(\boldsymbol{p}, t) \end{pmatrix}, \tag{7}$$

with

$$\boldsymbol{M}_2 = \begin{pmatrix} \chi(\boldsymbol{p}, t) & \chi^*(\boldsymbol{p}, t) \\ \psi(\boldsymbol{p}, t) & \psi^*(\boldsymbol{p}, t) \end{pmatrix}. \tag{8}$$

Here $\chi(\boldsymbol{p}, t)$ need not solve Eq. (3). If it does, the variables $a(\boldsymbol{p}, t)$ and $b^*(\boldsymbol{p}, t)$ are time-independent; otherwise, they acquire explicit time dependence to compensate for the evolution of $\chi(\boldsymbol{p}, t)$ and $\psi(\boldsymbol{p}, t)$, ensuring consistency of the field solution $\phi(\boldsymbol{p}, t)$ [61, 63]. The normalization condition

$$\chi(\boldsymbol{p}, t)\psi^*(\boldsymbol{p}, t) - \chi^*(\boldsymbol{p}, t)\psi(\boldsymbol{p}, t) = i, \tag{9}$$

ensures canonical commutation relations.

In canonical quantization,$a(\boldsymbol{p}, t)$ and $b^*(\boldsymbol{p}, t)$ are promoted to operators $\hat{a}(\boldsymbol{p}, t)$ and $\hat{b}^\dagger(\boldsymbol{p}, t)$ acting on Fock space. The vacuum state $|0\rangle_t$ is defined by $\hat{a}(\boldsymbol{p}, t)|0\rangle_t = 0$ for all $\boldsymbol{p}$. In the subsequent sections, we will use the hat notation exclusively for

quantum operators to distinguish them from their classical counterparts, which appear as c-number coefficients in the Bogoliubov transformations. This formalism demonstrates that a single classical theory can correspond to multiple quantized theories, each specified by different choices of $(\chi(\boldsymbol{p}, t), \psi(\boldsymbol{p}, t))$, which encode the quantization's complex structure [64].

The quantization procedure enforces unitarity through the field equations, reflecting the symmetries of the classical system. In Minkowski spacetime, Poincare symmetry uniquely fixes $\chi(\boldsymbol{p}, t)$ and $\psi(\boldsymbol{p}, t)$ as plane waves with frequency $\omega(\boldsymbol{p}, t)$. For slowly varying external fields, this framework extends via WKB-like solutions, recovering the Minkowski case when the frequency becomes approximately constant [5, 44, 65–67].

2.2 Parametrization in the mode function

The function $\chi(\boldsymbol{p}, t)$ can be approximated using a WKB-like ansatz [46, 61, 68]

$$\chi(\boldsymbol{p}, t) = \frac{1}{\sqrt{2\mathcal{W}(\boldsymbol{p}, t)}} e^{-i\Theta(\boldsymbol{p},t)}, \tag{10}$$

with two real functions: $\mathcal{W}(\boldsymbol{p}, t) > 0$(modulus) and $\Theta(\boldsymbol{p}, t)$ (phase), to be specified. Furthermore, it is straightforward to verify that the normalization condition reduces the non-uniqueness in the choice of the complex function $\psi(\boldsymbol{p}, t)$

$$\psi(\boldsymbol{p}, t) = -\sqrt{\frac{\mathcal{W}(\boldsymbol{p}, t)}{2}}[i + \mathcal{Y}(\boldsymbol{p}, t)]e^{-i\Theta(\boldsymbol{p},t)}. \tag{11}$$

Specific choices of $(\chi(\boldsymbol{p}, t), \psi(\boldsymbol{p}, t))$ are physically significant. In this particular case, one can insist that $\chi(\boldsymbol{p}, t)$ is a solution to the time-dependent differential equation (3) with time-dependent frequency $\mathcal{W}(\boldsymbol{p}, t)$, it is not only necessary for the normalization condition to be satisfied, but also for $\psi(\boldsymbol{p}, t) = \dot{\chi}(\boldsymbol{p}, t)$ [44, 64, 69]. This condition uniquely determines $\dot{\Theta}(\boldsymbol{p}, t)$ and $\mathcal{Y}(\boldsymbol{p}, t)$ as functions of $\mathcal{W}(\boldsymbol{p}, t)$, according to the relations:

$$\mathcal{W}(\boldsymbol{p}, t)^2 = \omega(\boldsymbol{p}, t)^2 - \frac{1}{2}\left[\frac{\ddot{\mathcal{W}}(\boldsymbol{p}, t)}{\mathcal{W}(\boldsymbol{p}, t)} - \frac{3}{2}\frac{\dot{\mathcal{W}}(\boldsymbol{p}, t)^2}{\mathcal{W}(\boldsymbol{p}, t)^2}\right], \tag{12}$$

$$\dot{\Theta}(\boldsymbol{p}, t) = \mathcal{W}(\boldsymbol{p}, t), \quad \mathcal{Y}(\boldsymbol{p}, t) = \frac{\dot{\mathcal{W}}(\boldsymbol{p}, t)}{2\mathcal{W}(\boldsymbol{p}, t)^2}. \tag{13}$$

Thus, the freedom in choosing the pair $(\chi(\boldsymbol{p}, t), \psi(\boldsymbol{p}, t))$, when imposing that $\chi(\boldsymbol{p}, t)$ is a specific normalized solution to the equation (3), is encoded in the initial conditions $\mathcal{W}(\boldsymbol{p}, t_0)$, $\dot{\mathcal{W}}(\boldsymbol{p}, t_0)$, and $\Theta(\boldsymbol{p}, t_0)$ at some initial time t_0.

Alternatively, one may require that $\chi(\boldsymbol{p}, t)$ is an approximate solution to the equation of motion. In this case, the equations for $\mathcal{W}(\boldsymbol{p}, t)$and $\mathcal{Y}(\boldsymbol{p}, t)$ hold approximately. For instance, when the time-dependent frequency $\omega(\boldsymbol{p}, t)$ varies slowly, the adiabatic approximation is commonly employed [61]. It can be viewed as a generalization of the WKB approximation, with the WKB approximation representing the zeroth order of the adiabatic expansion.

$$\mathcal{W}^{(0)}(\boldsymbol{p}, t) = \omega(\boldsymbol{p}, t), \Theta^{(0)}(\boldsymbol{p}, t) = \int_{t_0}^{t} dt'\, \omega(\boldsymbol{p}, t'). \tag{14}$$

For $\mathcal{Y}^{(0)}(\boldsymbol{p}, t)$, there are two possible choices, corresponding to different adiabatic orders (i.e., the number of time derivatives of $\omega(\boldsymbol{p}, t)$). The first choice, $\mathcal{Y}^{(0)}(\boldsymbol{p}, t) = \frac{\dot{\omega}(\boldsymbol{p}, t)}{2\omega(\boldsymbol{p}, t)^2}$, is frequently used in quantum field theory in curved spacetime [44, 45, 70]. This corresponds to approximating exact modes (called zeroth-order adiabatic modes) and their derivatives up to second-adiabatic order. The second choice, $\tilde{\mathcal{Y}}^{(0)}(\boldsymbol{p}, t) = 0$, is often employed in studies of quantum kinetic equation for particle production in the Schwinger mechanism and approximates exact adiabatic modes up to first-adiabatic order [25, 60, 67, 71, 72]. The implications of these two selections will be discussed in section 6.

In general, the n-th adiabatic approximation is obtained by recursively incorporating the previous order into the equation (12) for $\mathcal{W}(\boldsymbol{p}, t)$. The corresponding exact mode $f^{(n)}(\boldsymbol{p}, t)$, determined by the initial conditions $f^{(n)}(\boldsymbol{p}, t_0) = \chi^{(n)}(\boldsymbol{p}, t_0)$ and $\dot{f}^{(n)}(\boldsymbol{p}, t_0) = \psi^{(n)}(\boldsymbol{p}, t_0)$, is referred to as the n-th-order adiabatic mode. However, in general, $(\chi(\boldsymbol{p}, t), \psi(\boldsymbol{p}, t))$ are not required to be exact solutions of the equation of motion. Various alternative choices have been explored in the literature, including functions that diagonalize the Hamiltonian at large wave numbers[39] or those that minimize oscillations in the number of created particles over time [47, 73].

3 Dynamical quantity

3.1 Number of created particles

We compute the time-dependent particle number $\mathcal{N}(\boldsymbol{p}, t)$ via canonical transformations [60, 71, 72, 74]. We track $\mathcal{N}(\boldsymbol{p}, t)$ across vacuum states $|0\rangle_t$ and related to a reference vacuum $|0\rangle$. To analyze this evolution, we examine the behavior of the functions $\chi(\boldsymbol{p}, t)$ and $\psi(\boldsymbol{p}, t)$ over time, which describe the quantization process where particles are created or annihilated as time progresses.

To facilitate this, we first select a reference vacuum and fix a complex basis $(f(\boldsymbol{p}, t),\ f^*(\boldsymbol{p}, t))$ for the space of solutions to the Eq. (3) from which we define the associated creation and annihilation operators $\hat{a}(\boldsymbol{p})$ and $\hat{b}^\dagger(\boldsymbol{p})$, which remain time-independent. The reference vacuum, denoted by $|0\rangle$, is defined as the state annihilated by $\hat{a}(\boldsymbol{p})$ operator. This formulation allows us to study the evolution of the particle number and its dependence on the choice of vacuum state. The different sets of annihilation and creation variables, $(\hat{a}(\boldsymbol{p}),\ \hat{b}^\dagger(-\boldsymbol{p}))$ and $(\hat{a}(\boldsymbol{p}, t),\ \hat{b}^\dagger(-\boldsymbol{p}, t))$, which are associated with the basis functions $(f(\boldsymbol{p}, t),\ f^*(\boldsymbol{p}, t))$ and $(\chi(\boldsymbol{p}, t),\ \psi(\boldsymbol{p}, t))$, are related through a canonical transformation known as the Bogoliubov transformation $\mathcal{B}(t)$. The $\boldsymbol{p}$-component of this transformation, denoted $\mathcal{B}(\boldsymbol{p}, t)$, is expressed as

$$\begin{pmatrix} \hat{a}(\boldsymbol{p},t) \\ \hat{b}^\dagger(-\boldsymbol{p},t) \end{pmatrix} = \mathcal{B}(\boldsymbol{p},t) \begin{pmatrix} \hat{a}(\boldsymbol{p}) \\ \hat{b}^\dagger(-\boldsymbol{p}) \end{pmatrix}, \tag{15}$$

The Bogoliubov transformation $\mathcal{B}(\boldsymbol{p}, t)$ relates annihilation/creation operators between bases.

$$\mathcal{B}(\boldsymbol{p},t) = \begin{pmatrix} \alpha(\boldsymbol{p},t) & \beta^*(\boldsymbol{p},t) \\ \beta(\boldsymbol{p},t) & \alpha^*(\boldsymbol{p},t). \end{pmatrix} \tag{16}$$

Unitarity preserves commutation relations, enforcing

$$|\alpha(\boldsymbol{p},t)|^2 - |\beta(\boldsymbol{p},t)|^2 = 1. \tag{17}$$

The Bogoliubov transformation (16) offers a clearer understanding of the physical implications of choosing annihilation and creation operators, as noted in the literature [74, 75]. In this context, the time-dependent particle number $\mathcal{N}(\boldsymbol{p}, t)$ is defined for each mode $\boldsymbol{p}$ in the quantum theory, which is characterized by the set $(\hat{a}(\boldsymbol{p}, t),\ \hat{b}^\dagger(-\boldsymbol{p}, t))$. This particle number is measured with respect to the reference vacuum state $|0\rangle$, and is expressed as:

$$\begin{aligned} \mathcal{N}(\boldsymbol{p},t) &= \langle 0|\hat{a}(\boldsymbol{p},t)^\dagger \hat{a}(\boldsymbol{p},t)|0\rangle = \langle 0|\hat{b}^\dagger(-\boldsymbol{p},t)\hat{b}(-\boldsymbol{p},t)|0\rangle \\ &= |\beta(\boldsymbol{p},t)|^2. \end{aligned} \tag{18}$$

In the last step, we used the fact that the vacuum is annihilated by the original creation and annihilation operators, $\hat{a}(\boldsymbol{p})|0\rangle = 0$, and $\hat{b}(-\boldsymbol{p})|0\rangle = 0$, under the assumption that no particles were initially present [72]. The total number of particles created in mode $\boldsymbol{p}$ is given by the final value of $\mathcal{N}(\boldsymbol{p}, t)$:

$$\mathcal{N}(\boldsymbol{p}, t = +\infty) = |\beta(\boldsymbol{p}, t = +\infty)|^2. \tag{19}$$

Consequently, $\mathcal{N}(\boldsymbol{p}, t)$ can be interpreted as the number of real particles only at asymptotic times, when the external field is switched off (or, vanished). Alternative interpretations that overlook this peculiarity of $\mathcal{N}(\boldsymbol{p}, t)$ can lead to surprisingly unconventional results [49, 75].

In this work, we focus on the complete time evolution of the particle number $\mathcal{N}(\boldsymbol{p}, t)$, tracing its progression from an initial value of zero to a final asymptotic value $\mathcal{N}(\boldsymbol{p}, t = +\infty)$.

The Bogoliubov coefficients are derived from the classical equivalence of $\phi(\boldsymbol{p}, t)$ and $\pi(\boldsymbol{p}, t)$ in Eqs. (5) and (7). We finally deduce that

$$\begin{aligned} \begin{pmatrix} \alpha(\boldsymbol{p},t) \\ \beta^*(\boldsymbol{p},t) \end{pmatrix} &= M^{-1} \begin{pmatrix} f(\boldsymbol{p},t) \\ \dot{f}(\boldsymbol{p},t), \end{pmatrix} \\ M^{-1}(t) &= i \begin{pmatrix} \psi^*(\boldsymbol{p},t) & -\chi(\boldsymbol{p},t) \\ -\psi(\boldsymbol{p},t) & \chi(\boldsymbol{p},t) \end{pmatrix}. \end{aligned} \tag{20}$$

The particle number $\mathcal{N}(\boldsymbol{p}, t)$ is expressed via the Bogoliubov coefficient $|\beta(\boldsymbol{p}, t)|^2$ and the mode functions:

$$\begin{aligned} |\beta(\boldsymbol{p},t)|^2 &= |\psi(\boldsymbol{p},t)|^2 |f(\boldsymbol{p},t)|^2 - \dot{f}(\boldsymbol{p},t)[\psi\chi^*(\boldsymbol{p},t) f(\boldsymbol{p},t) + \psi^*(\boldsymbol{p},t)\chi(\boldsymbol{p},t) f^*(\boldsymbol{p},t)] \\ &\quad + |\chi(\boldsymbol{p},t)|^2 |\dot{f}(\boldsymbol{p},t)|^2. \end{aligned} \tag{21}$$

Also, one can now express $\mathcal{N}(\boldsymbol{p}, t)$ in terms of the functions $\mathcal{W}(\boldsymbol{p}, t)$,$\Theta(\boldsymbol{p}, t)$, and $\mathcal{Y}(\boldsymbol{p}, t)$, which characterize $\chi(\boldsymbol{p}, t)$ and $\psi(\boldsymbol{p}, t)$, and the exact mode solution $f(\boldsymbol{p}, t)$ that defines the reference vacuum $|0\rangle$:

$$\begin{aligned} \mathcal{N}(\boldsymbol{p},t) &= \frac{\mathcal{W}(\boldsymbol{p},t)}{2}\left[1 + \mathcal{Y}(\boldsymbol{p},t)^2\right]|f(\boldsymbol{p},t)|^2 + \frac{1}{2\mathcal{W}(\boldsymbol{p},t)}|\dot{f}(\boldsymbol{p},t)|^2 \\ &\quad - \frac{1}{2} + \mathcal{Y}(\boldsymbol{p},t)\Re f^*(\boldsymbol{p},t)\dot{f}(\boldsymbol{p},t). \end{aligned} \tag{22}$$

This result generalizes the expression found in [58, 76], which corresponds to the specific case where we choose $(\chi(\boldsymbol{p}, t),\ \psi(\boldsymbol{p}, t))$ as the zeroth-order adiabatic approximation $(\chi^{(0)}(\boldsymbol{p}, t),\ \psi^{(0)}(\boldsymbol{p}, t))$, fixed by (14) and $\mathcal{Y}^{(0)}(\boldsymbol{p}, t) = 0$:

$$\mathcal{N}^{(0)}(\boldsymbol{p},t) = \frac{\omega(\boldsymbol{p},t)}{2}|f(\boldsymbol{p},t)|^2 + \frac{1}{2\omega(\boldsymbol{p},t)}|\dot{f}(\boldsymbol{p},t)|^2 - \frac{1}{2}. \tag{23}$$

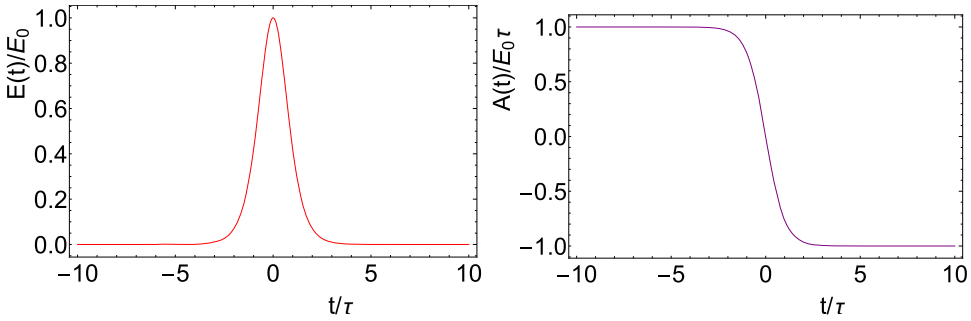

Fig. 2 Temporal profile of the electric field (28) (left) and the corresponding vector potential with the choice $A(t=0)=0$ (right) and all the units are taken in the electron mass unit

Here, $f(\boldsymbol{p}, t)$ is the zeroth-order adiabatic mode (initial conditions at t_0), and Eq. (23) matches the quantum kinetic formalism [72, 74].

3.2 Correlation function

The correlation function $\mathcal{C}(\boldsymbol{p}, t)$ captures pair creation/annihilation dynamics tied to $\mathcal{N}(\boldsymbol{p}, t)$. Consequently, it is necessary to define a term that captures these creation and annihilation processes. The pair correlation function $\mathcal{C}(\boldsymbol{p}, t)$ quantifies vacuum fluctuations:

$$\mathcal{C}(\boldsymbol{p},t) = \langle 0|\hat{a}^{\dagger}(\boldsymbol{p},t)\hat{b}^{\dagger}(-\boldsymbol{p},t)|0\rangle \tag{24}$$

and its complex conjugate

$$\mathcal{C}^{*}(\boldsymbol{p},t) = \langle 0|\hat{a}(\boldsymbol{p},t)\hat{b}(-\boldsymbol{p},t)|0\rangle \tag{25}$$

This function $\mathcal{C}(\boldsymbol{p}, t)$ consisting of creation operators for a particle and an anti-particle with the opposite momentum describes the process of creation of pairs.

Calculating the expectation value and doing the limiting procedure one can find [74, 77]

$$\mathcal{C}(\boldsymbol{p},t) = \alpha(\boldsymbol{p},t)\beta^{*}(\boldsymbol{p},t) \tag{26}$$

In terms of $\mathcal{W}(\boldsymbol{p}, t)$ and $\mathcal{Y}(\boldsymbol{p}, t)$, the correlation function becomes:

$$\begin{aligned}\mathcal{C}(\boldsymbol{p},t) = \frac{\mathcal{W}(\boldsymbol{p},t)}{2}\Big[1-\mathcal{Y}^{2}(\boldsymbol{p},t)+2\mathrm{i}\mathcal{Y}(\boldsymbol{p},t)\Big]|f(\boldsymbol{p},t)|^{2}-\frac{1}{2\mathcal{W}(\boldsymbol{p},t)}|\dot{f}(\boldsymbol{p},t)|^{2}\\ +\frac{1}{2}(\mathrm{i}-\mathcal{Y}(\boldsymbol{p},t))\Big[f(\boldsymbol{p},t)\dot{f}^{*}(\boldsymbol{p},t)+f^{*}(\boldsymbol{p},t)\dot{f}(\boldsymbol{p},t)\Big].\end{aligned} \tag{27}$$

4 Sauter-pulse electric field

A spatially uniform external background is often used as an approximation for the electromagnetic field near the focal region of two counter-propagating laser pulses along the z-axis, forming a standing wave [56, 78]. In general, pair production occurs near the peak of the electric field–comparable to the critical field limit–where the magnetic field vanishes. Although laser fields typically consist of many optical cycles, we consider a simplified model where the external field follows a Sauter profile, representing an extremely short laser pulse.

$$E(t) = E_0 \mathrm{sech}^{2}\left(\frac{t}{\tau}\right), \tag{28}$$

where τ is the pulse duration and E_0 is the field strength. This electric field decays exponentially to zero for $|t| \gg \tau$. In the limit $\tau \to \infty$, the field becomes homogeneous in time. Choosing a gauge where $A_0 = 0$, the vector potential corresponding to this electric field is given by:

$$A(t) = -E_0\tau \tanh\left(\frac{t}{\tau}\right), \tag{29}$$

The left panel of Fig. 2 illustrates the temporal profile of the electric field in Eq. (28).

Sauter [4] originally analyzed the Dirac equation in the presence of an inhomogeneous scalar potential of the form $V(z) = V_0\,\mathrm{sech}^{2}(z/d)$. Since this problem reduces to a one-dimensional differential equation, a similar approach applies when the potential varies in time, as in Eq. (28). The vacuum instability induced by a time-dependent Sauter-like electric field was first studied by Narozhny et al. in 1970 [50]. Since then, numerous works have revisited this topic, employing various theoretical approaches–including approximate methods–within this framework. Notable examples include Refs. [52, 54] and references therein.

Now, Eq. (3) can be rewritten in the presence of electric field Eq.(28)

$$\ddot{f}(\boldsymbol{p},t)+\omega^2(\boldsymbol{p},t)f(\boldsymbol{p},t)=0, \tag{30}$$

where,

$$\omega(\boldsymbol{p},t)=\sqrt{\left(p_{\parallel}-eE_0\tau\tanh\left(\frac{t}{\tau}\right)\right)^2+p_{\perp}^2+m^2}. \tag{31}$$

This equation can be solved by converting it into a hypergeometric differential equation [79], by changing the time variable to $y=\frac{1}{2}\left(1+\tanh\left(\frac{t}{\tau}\right)\right)$.

The new variable y transforms the equation as

$$\left[\frac{4}{\tau^2}y(1-y)\frac{d}{dy}\,y(1-y)\frac{d}{dy}+\omega^2(\boldsymbol{p},y)\right]f(\boldsymbol{p},y)=0. \tag{32}$$

In this case, solutions can be written in terms of hypergeometric functions [79] :

$$f(\boldsymbol{p},y)=\frac{1}{\sqrt{2\omega_0}}y^{-i\tau\omega_0/2}(y-1)^{i\tau\omega_1/2}{}_2F_1(a,b,c;y) \tag{33}$$

where, ${}_2F_1(a,\,b,\,c;y)$ is the hypergeometric function, and

$$\begin{aligned}
a=&\frac{1}{2}+\frac{i}{2}(\tau\omega_1-\tau\omega_0)-i\lambda,\\
b=&\frac{1}{2}+\frac{i}{2}(\tau\omega_1-\tau\omega_0)+i\lambda,\\
c=&1-i\tau\omega_0,\\
\lambda=&\sqrt{(eE_0\tau^2)^2-\frac{1}{4}},\\
\omega_0=&\sqrt{(p_{\parallel}+eE_0\tau)^2+p_{\perp}^2+m^2},\\
\omega_1=&\sqrt{(p_{\parallel}-eE_0\tau)^2+p_{\perp}^2+m^2}.
\end{aligned} \tag{34}$$

We reduce to (1+1)D by setting $p_{\perp}=0$ and $p_{\parallel}\equiv p$, simplifying the analysis.

From Eq. (23), the time-dependent particle number for each mode p is given by

$$\mathcal{N}(p,t)=\frac{1}{4\omega_0\mathcal{W}(p,t)}\left|\frac{2}{\tau}y(1-y)\frac{ab}{c}g_1+\mathrm{i}(\mathcal{W}(p,t)(\mathrm{i}+\mathcal{Y}(p,t))-(1-y)\omega_0-y\omega_1)g_2\right|^2 \tag{35}$$

where, $g_1={}_2F_1(1+a,\,1+b,\,1+c;y)$, $g_2={}_2F_1(a,\,b,\,c;y)$.

5 Numerical results

We investigate the dynamical behavior of the key quantities governing pair production, as introduced in Section 3. For this purpose, we adopt the natural choice $\mathcal{W}(p,\,t)=\omega(p,\,t)$ and $\mathcal{Y}(p,\,t)=0$, a convention widely used in the literature on the quantum kinetic equation for pair creation in intense laser fields [67, 71, 72].

5.1 Vacuum polarization function

A more fundamental description of pair creation dynamics is provided by the correlation function $\mathcal{C}(p,\,t)$ as discussed in Sec. 3.2. Its decomposition into real and imaginary parts,

$$\mathcal{C}(p,t)=u(p,t)+iv(p,t), \tag{36}$$

where $u(p,\,t)=\mathrm{Re}[\mathcal{C}(p,\,t)]$ and $v(p,\,t)=\mathrm{Im}[\mathcal{C}(p,\,t)]$, reveals two physically distinct aspects of the vacuum's response [74, 80].

The function $u(p,t)$ characterizes the instantaneous vacuum polarization, representing the coherent fluctuations of virtual particle-antiparticle pairs aligned by the external field. It quantifies the degree to which the quantum vacuum becomes electrically polarized. Its counterpart, $v(p,\,t)$, governs the depolarization dynamics, acting as a counter-term that encapsulates the vacuum's reactive response. These functions form a coupled dynamical system [56],

$$\dot{u}(p,\,t)\propto -v(p,\,t),\quad \dot{v}(p,\,t)\propto u(p,\,t),$$

illustrating that the growth of vacuum polarization is accompanied by a restoring response. This interplay is central to understanding the polarization current.

As discussed in Subsect. 3.2, the vacuum polarization effects can be described by the functions $u(p, t)$ and $v(p, t)$ [57, 81]. Both of these components originate from correlation functions as defined in Eq. (26).

In the presence of an intense Sauter pulsed field ((28)), we compute the vacuum polarization function using the exact solution of the mode function (37), given by

$$u(p,t) = \frac{2}{\tau\omega_0}|\frac{ab}{c}|^2|\frac{\tau}{2}\Big(\frac{-ic}{ab}\Big)[\omega_0(1-y)+\omega_1 y]g_1 + y(1-y)g_2|^2 - \frac{1}{2\omega_0}\mathcal{W}(p,t)(\mathcal{W}(p,t)^2 - \mathcal{Y}(p,t)^2)$$
$$+ \mathcal{Y}(p,t)\mathcal{W}(p,t)\frac{2}{\tau\omega_0}y(1-y)\Re(\frac{ab}{c}g_1^* g_2) \tag{37}$$

whereas the corresponding counter-term

$$v(p,t) = \frac{-1}{\omega_0}\mathcal{W}(p,t)^2\mathcal{Y}(p,t)|g_1|^2 + y(1-y)\frac{1}{\tau\omega_0}\mathcal{W}(p,t)\Re(\frac{ab}{c}g_1^* g_2) \tag{38}$$

To analyze the dynamical behavior of the polarization functions $u(p, t)$ and $v(p, t)$, we first fix the freedom in choosing ($\mathcal{W}(p, t)$, $\mathcal{Y}(p, t)$). Following our previous approach, we adopt the natural choice $\mathcal{W}(p, t) = \omega(p, t)$ and $\mathcal{Y}(p, t) = 0$.

Now, Eqs. (37)–(38) simplified as

$$u(p,t) = \frac{2}{\tau\omega_0}\left|\frac{ab}{c}(y(\omega_1-\omega_0)+\omega_0)\right|^2\Bigg[\left|\frac{y(1-y)}{(\omega_1-\omega_0)y+\omega_0}g_2\right|^2 - \left|\frac{\tau c}{2ab}g_1\right|^2$$
$$- 2\Re\Big(\frac{y(1-y)}{y(\omega_1-\omega_0)+\omega_0}\frac{\tau c}{2ab}g_1 g_2^*\Big)\Bigg] - \frac{1}{2\omega_0}\omega(p,t)^3|g_2|^2, \tag{39}$$

and,

$$v(p,t) = y(1-y)\frac{\omega(p,t)}{\tau\omega_0}\Re(\frac{ab}{c}g_1^* g_2). \tag{40}$$

For a better understanding of the phenomenon of particle creation under a strong electric field, we will also trace the evolution of the vacuum polarization function $u(p, t)$, and its counter-term $v(p, t)$, which governs the depolarization. At early times $t < \tau$, $u(p, t) \approx 0$, confirming the system begins in a stable vacuum state before field interaction. A sharp peak emerges at $t = 0$, maximized at $p = 0$ for $u(p, t)$ (dashed red) and $p = -1$ for $v(p, t)$ (see Fig. 3).The structure of these peaks varies with momentum, reflecting the momentum dependence of the response. The insert of Fig. 3a reveals residual oscillations that persist in late times where the field vanishes and the real particle-antiparticle are produced from the vacuum. The amplitude of oscillation is higher for a lower momentum ($p = 0$) value and oscillates about the origin. As shown in Fig. 5b, $v(p, t)$ is antisymmetric in t. The function starts from zero at early times as similar to $u(p, t)$. For $p = 0$ (red dashed),$v(p, t)$ is antisymmetric about $t = 0$, with a positive peak at $t > 0$ mirroring a negative peak at $t < 0$. The central peak for $p = 0$ (red dashed line) is symmetric about $t = 0$, but in an antisymmetric manner: its positive peak for $t > 0$ corresponds to a negative counterpart for $t < 0$ For $p = 1$ (brown) and $p = -1$ (purple), the structure remains antisymmetric, with one curve being a mirror image (with a sign flip) of the other. As seen in the function $u(p, t)$ in asymptotic time, the oscillatory behavior is observed as seen in the insert of Fig. 3b.

Early-time dynamics favor pair annihilation over creation, reflected in the larger amplitude of $v(p, t)$ compared to $u(p, t)$. This is evident from the larger amplitudes of $v(p, t)$ compared to $u(p, t)$ during the early evolution stage. Both functions exhibit oscillations with varying amplitudes. The oscillations are particularly strong for $p = 0$, as shown in the insets of the plots. The peak-like structure in $u(p, t)$ likely arises from interference between vacuum fluctuations and field-driven pair creation. In contrast to $u(p, t)$, $v(p, t)$ displays antisymmetric peaks. Transient-stage oscillations are irregular, a signature of non-equilibrium pair production/annihilation dynamics. At late times, the system equilibrates, with oscillations regularizing and centering at zero. Late-time oscillations in $u(p, t)$ and $v(p, t)$ converge, indicating equilibrium between polarization and depolarization. This behavior mirrors that of spin-1/2 fermions [77, 80].

We now analyze how the field strength E_0 influences the polarization functions $u(p, t)$ and $v(p, t)$. Figure 4 shows the time dependence of $u(p, t)$ and $v(p, t)$ for varying E_0.With increasing E_0, the peak amplitudes of $u(p, t)$ and $v(p, t)$ near $t \approx 0$ grow, reflecting enhanced transient dynamics. Oscillations emerge earlier and amplify for $E_0 = 0.3E_c$, signaling stronger dynamical evolution. The late-time behavior reveals oscillations, whose amplitude and duration increase with field strength. The behavior of the polarization function $u(p, t)$ and its counterterm $v(p, t)$ is also influenced by the pulse duration τ. The pulse duration τ also modulates $u(p, t)$ and $v(p, t)$. At $t \approx 0$, $u(p, t)$ peaks maximally for the shortest pulse ($\tau = 5$), while $v(p, t)$ peaks for the longest ($\tau = 25$) (Fig. 5(a, b)). In the asymptotic regime, both functions oscillate with smaller amplitudes for $\tau = 5$ than for $\tau = 25$.

The distinct behaviors of $u(p, t)$ and $v(p, t)$–the symmetric polarization and antisymmetric depolarization response–provide a complete picture of the vacuum's coherent dynamics. Their evolution is directly tied to the observable polarization current, which we examine in the next Sect. 5.2.

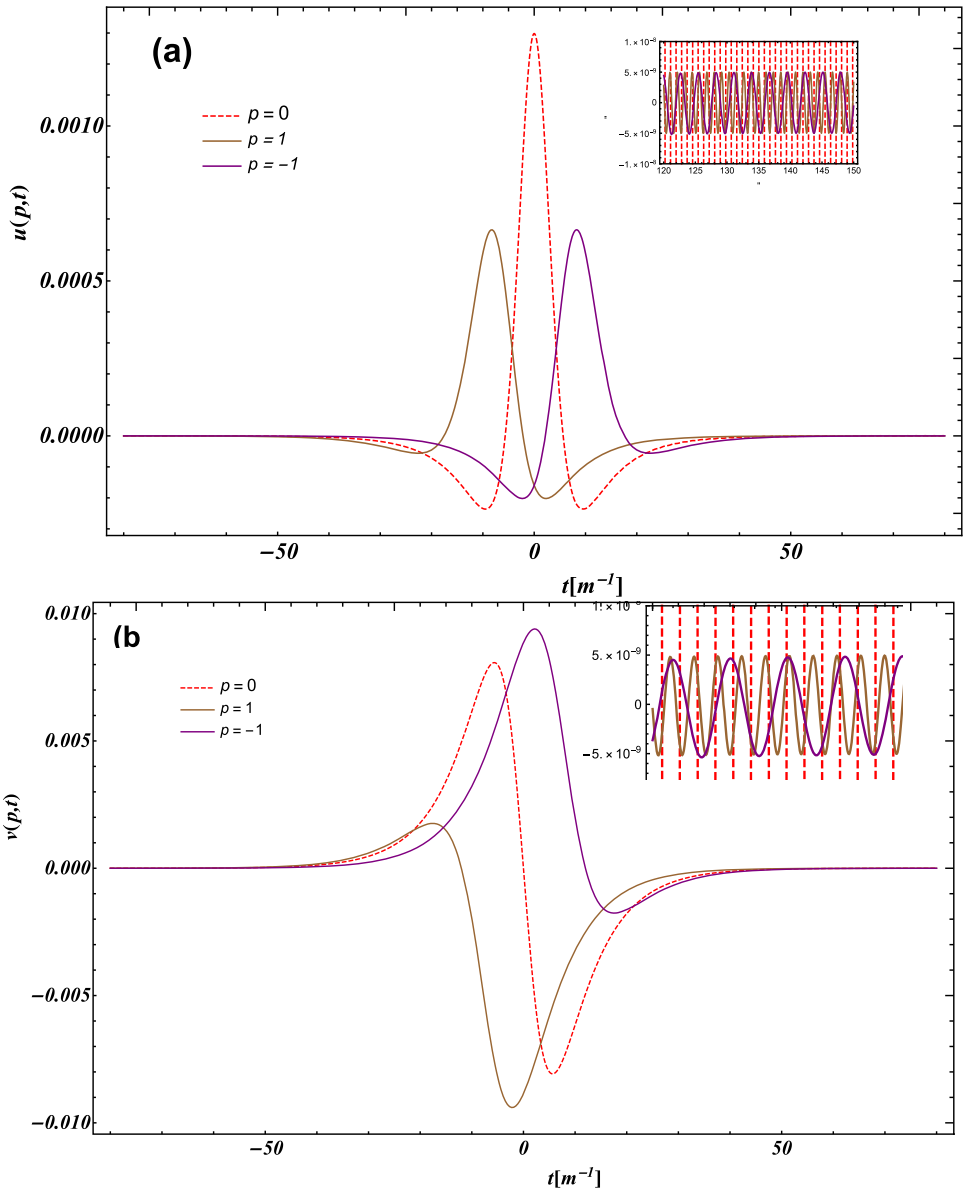

Fig. 3 **Upper panel:** Evolution of $u(t)$ and **Lower panel:** Evolution of $v(t)$ for different momentum value p. All the units are taken in electron mass unit. The field parameters are $E_0 = 0.1E_c$ and $\tau = 15[m^{-1}]$

While our focus is on the correlation functions, it is instructive to briefly examine the behavior of the particle number $\mathcal{N}(p,\, t)$ in the same conventional basis to contextualize its limitations.

To explore the dynamical behavior of $\mathcal{N}(p,\, t)$ for natural choice $\mathcal{W}(p,\, t) = \omega(p,\, t)$ and $\mathcal{Y}(p,\, t) = 0$, frequently used in studies of pair creation from intense laser fields. With this choice, the particle number $\mathcal{N}(p,\, t)$ is given by

$$\mathcal{N}(p,t) = \frac{1}{4\omega_0\omega(p,t)}\Bigg(\Big|\frac{2}{\tau}y(1-y)\frac{ab}{c}g_1\Big|^2 + \Big|((\omega_0 + \mathrm{i}\omega(p,t)) + y(\omega_1 - \omega_0))g_2\Big|^2$$
$$+ \frac{4}{\tau}y(1-y)\Re\Big(\frac{ab}{c}g_1((\omega_0 - \mathrm{i}\omega(p,t)) + y(\omega_1 - \omega_0))g_2^*\Big)\Bigg) \tag{41}$$

Figure 6 shows $\mathcal{N}(p,\, t)$ for the same parameters as in Figs. 4, 5. The time evolution of $\mathcal{N}(p,\, t)$ reflects the creation of quasiparticles–transient, field-dressed excitations that are not yet on-shell real particles [74]. A key observation from this comparison is that the magnitude of $\mathcal{N}(p,\, t)$ remains very low compared to the amplitudes of the polarization functions $u(p,\, t)$ and $v(p,\, t)$ throughout the main interaction period (for the parameters shown). This indicates that the population of these quasiparticles is strongly suppressed while the external field is active. It is only at asymptotic times, long after the field has vanished and these quasiparticles have decoupled to become real particles, that $\mathcal{N}(p,\, t)$ saturates to a finite value. However, during the crucial dynamics of the pair creation process, the system is dominated by the coherence of particle-antiparticle and polarization captured by $u(p,\, t)$ and $v(p,\, t)$, which

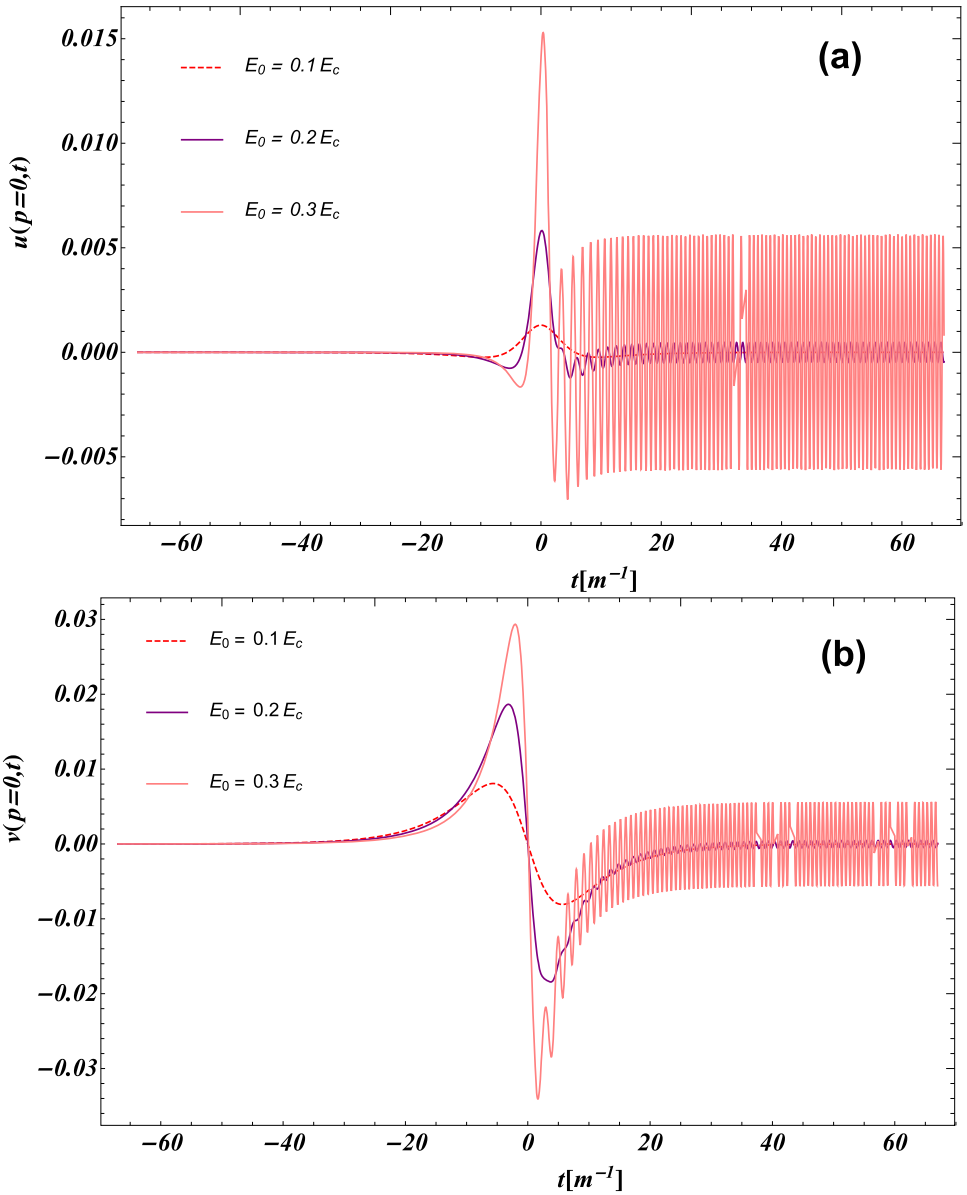

Fig. 4 Upper panel : Evolution of $u(t)$ and **Lower panel :** Evolution of $v(t)$ for different field strengths E_0. All the units are taken in electron mass unit. The momentum is considered to be zero, and pulse duration, $\tau = 15[m^{-1}]$

maintain large amplitudes. This observation has a direct and important consequence for the physical currents that will be derived in Sect. 5.2.

5.2 Vacuum polarization current

The physical current induced by the external field is given by the expectation value of the spatial component of the gauge-invariant Noether current. For completeness, we discuss this procedure–although it has been discussed in refs. [60, 61]–and outline the essential steps here to make the presentation self-contained.

The conserved current associated with the global $U(1)$ symmetry of a complex scalar field $\Phi(t, \boldsymbol{x})$ follows from Noether's theorem [82, 83],

$$\hat{j}_\mu = ie\Big[\Phi^\dagger(\partial_\mu + ieA_\mu)\Phi - (\partial_\mu - ieA_\mu)\Phi^\dagger\Phi\Big], \tag{42}$$

This is the definition of the current operator.

Taking the expectation value of the spatial component of this operator in the vacuum state gives the electric current (or physical observable in general),

$$j^z(t) = \langle 0|\, \hat{j}_3(t)\, |0\rangle. \tag{43}$$

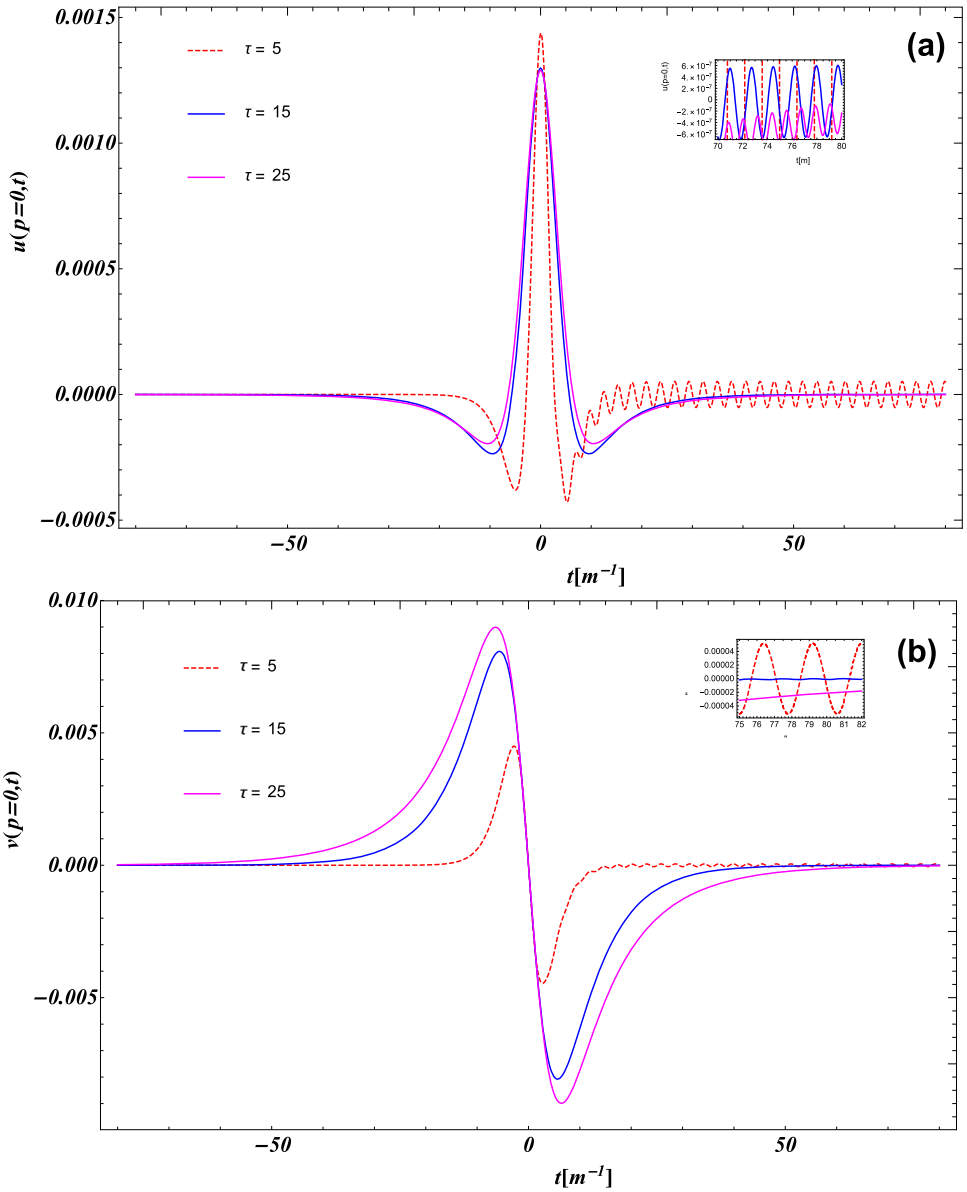

Fig. 5 **Upper panel :**Evolution of $u(t)$ and **Lower panel :**Evolution of $v(t)$ for different pulse duration. The momentum is considered to be zero, and field strength, $E_0 = 0.1E_c$

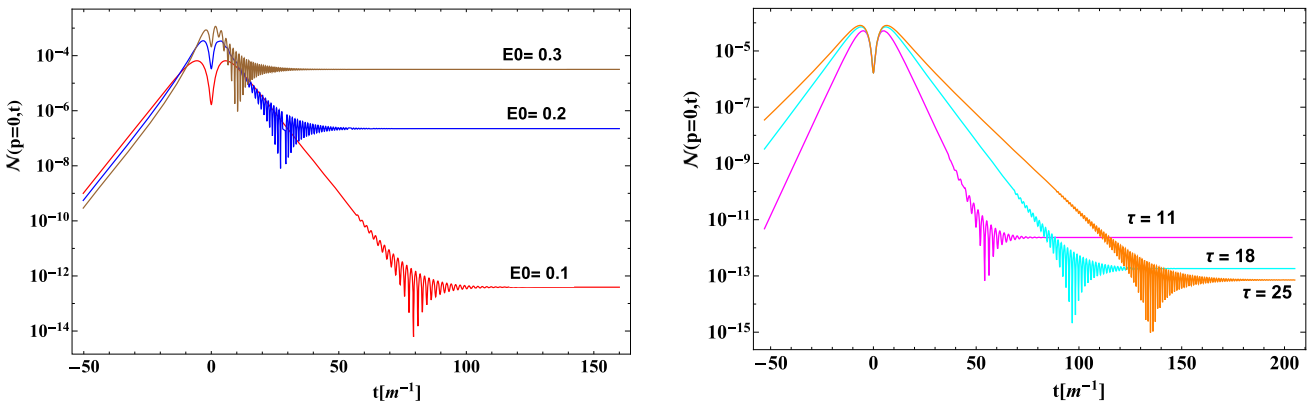

Fig. 6 Left panel: Evolution of $\mathcal{N}(p,\, t)$ for different field strengths $E_0 = 0.1E_c$ (red), $0.2\mathrm{E_c}$ (blue), $0.3\mathrm{E_c}$ (brown), and $\tau = 15[\mathrm{m}^{-1}]$. Right panel: Evolution of $\mathcal{N}(p,\, t)$ for different pulse durations $\tau = 11[\mathrm{m}^{-1}]$ (magenta), $18[\mathrm{m}^{-1}]$ (cyan), $25[\mathrm{m}^{-1}]$ (orange), and $E_0 = 0.1E_c$. The momentum is considered to be zero, and all quantities are expressed in units of the electron mass

In 1 + 1 dimensions, the temporal component ($\mu = 0$) vanishes, meaning that no net charge is produced [54, 84].

In our spatially homogeneous, time-dependent electric field setup, the relevant physical quantity is the spatially averaged current density along the field direction. After decomposing the field into Fourier modes and assuming no initial particles, the expectation value of the current density is given by

$$j^z(t) = e \int \frac{dp}{2\pi} \, (p - eA(t)) \, |f(p,t)|^2. \tag{44}$$

The current $j^z(t)$ is composed of three distinct parts that carry different physical origin [85–87].Using the linear transformation to the adiabatic basis

$$f(p,t) = \alpha(p,t)\,\chi(p,t) + \beta(p,t)\,\chi^*(p,t), \tag{45}$$

where $\chi(p,\, t)$ given by the relation Eq.(10).

Substituting this into Eq. (44) gives

$$j^z(t) = 2e \int \frac{dp}{2\pi} \frac{(p - eA(t))}{\omega(p,t)} \Big[\frac{1}{2} + \mathcal{N}(p,t) + u(p,t)\Big], \tag{46}$$

where $\mathcal{N}(p,\, t) = |\beta(p,\, t)|^2$ is the particle number and polarization function $u(p,\, t) = \mathrm{Re}[\mathcal{C}(p,\, t)]$. The first term in Eq. (46) is independent of $\mathcal{N}(p,\, t)$and $u(p,\, t)$ and arises solely from the background vacuum,

$$j_{\mathrm{vac}}(t) = e \int \frac{dp}{2\pi} \frac{(p - eA(t))}{\omega(p,t)}. \tag{47}$$

This contribution reflects the vacuum fluctuations. It does not correspond to any measurable effect and therefore must be subtracted to obtain the physically meaningful current [88]. In this sense, the only meaningful definition of the total induced current is

$$J(t) = j^z(t) - j_{\mathrm{vac}}(t). \tag{48}$$

Carrying out this subtraction gives

$$J(t) = J_{\mathrm{cond}}(t) + J_{\mathrm{pol}}(t), \tag{49}$$

where

$$J_{\mathrm{cond}}(t) = 2e \int \frac{dp}{2\pi} \frac{(p - eA(t))}{\omega(p,t)} \mathcal{N}(p,t), \tag{50}$$

$$J_{\mathrm{pol}}(t) = 2e \int \frac{dp}{2\pi} \frac{(p - eA(t))}{\omega(p,t)} u(p,t). \tag{51}$$

The total current $J(t)$, therefore, consists of two physically distinct contributions: The conduction current, $J_{\mathrm{cond}}(t)$, is proportional to the instantaneous particle number ($\mathcal{N}(p,\, t)$). It represents the current carried by real, on-shell particles that have been created. The polarization current, $J_{\mathrm{pol}}(t)$, originates from quantum correlations between particle–antiparticle states and describes the instantaneous polarization of the vacuum in the presence of the field.

The crucial observation is that while the separation in Eq.(49) depends on the choice of the adiabatic basis functions ($\chi(p,\, t)$, $\psi(p,\, t)$), the total induced current $J(t)$ does not. Since $J(t)$ is defined from the renormalized Noether current, it is a basis-independent physical observable.

During the early and intermediate stages of the pair production process, when the field is strong, the number of real, asymptotic particles is small and ill-defined. This is reflected in the basis-dependence of $\mathcal{N}(p,\, t)$ (see the next Sect. 6). In this regime, the total current is dominated by the polarization component. Since $J(t)$ is basis-independent, it follows that the polarization current $J_{\mathrm{pol}}(t)$ itself must be largely unaffected by the choice of adiabatic basis during the field's presence. It is not merely one part of a decomposition, but rather the physical observable itself at intermediate times. Therefore, it is important to analysis and explore the dynamical properties of the vacuum polarization current, which depends on the polarization function $u(p,\, t)$.

The polarization current can be explicitly written as

$$J_{pol.}(t) = \frac{e}{\pi} \int dp \frac{(p - eA(t))}{\omega(p,t)} u(p,t). \tag{52}$$

We first examine the integrand of $J_{pol.}(t)$ (see Eq. (52)) before performing the integration to gain a better understanding of the behavior of the polarization current. Through this, one can see the relationship between the polarization response and momentum.

Figure 7 illustrates the time evolution of the integrand of the polarization current $J_{pol.}(t)$ (blue) and the polarization function $u(p,t)$ (red) for different momentum values p. The analysis is conducted for the field parameters $E_0 = 0.1E_c$ and $\tau = 15[m^{-1}]$. Before the field becomes significant, both the integrand of polarization current and $u(p,\, t)$ are close to zero for $t << -2\tau$. This indicates that there is no significant particle excitation in the system yet. The integrand of $J_{pol.}(t)$ and $u(p,\, t)$ both exhibit a well-defined peak structure, with the strongest response around $t = 0[m^{-1}]$, corresponding to the peak of the field. The polarization current integrand shows a distinct oscillatory structure around the central peak. The function $u(p,\, t)$ follows a similar trend but exhibits a sharper

peak. The blue curve, which involves the momentum-dependent prefactor, follows a similar trend of $u(p, t)$ but is modulated by $\frac{(p-eA(t))}{\omega(p,t)}$. In the later time, $t > \tau$, the electric field vanishes, and $A(t)$ asymptotically approaches a constant value. The integrand of $J_{pol.}(t)$ in this time exactly follows the behavior of $u(p, t)$, which exhibits regular oscillations about the origin. We also point out that as the momentum value increases ($p = 2$, 4 in the middle and right panels), the amplitude of both curves decreases, and the peak position shifts slightly, reflecting a momentum-dependent delay in the response. The time evolution of the integrand of $J_{pol.}(t)$ and $u(p, t)$ for $p = 4$ (see right panel) shows that both curves nearly overlap, indicating that at higher momentum, the integrand of $J_P(t)$ behaves similarly to the function $u(p, t)$. This can be understood as, for higher momentum values ($p \gg eA(t)$), the prefactor becomes negligible, and the integrand is dominated by $u(p, t)$.

To demonstrate the dependence on the pulse duration τ, we plot for $\tau = 5$ and compare with Fig. 7 in the Fig. 8. For the shorter pulse duration, the integrand of $J_{pol.}(t)$ (blue curve) exhibits more pronounced oscillations at $t > 0$, particularly for smaller momenta. This is because a shorter pulse contains a broader frequency spectrum. The peak values are reduced compared to $\tau = 15[m^{-1}]$, indicating that the system has less time to develop a strong response. The functions decay more quickly after the field pulse, meaning the system returns to equilibrium faster. As seen in the right panel of Fig. 8, for $p = 4$, the blue and red curves nearly overlap, similar to the $\tau = 15[m^{-1}]$ case. This indicates that at higher momentum, the behavior of the integrand of $J_P(t)$ remains dominated by $u(p, t)$ regardless of pulse duration. The regular oscillations at asymptotic times, after the field ceases, are observed with an increased frequency compared to the previous pulse duration.

Now, to calculate the integration for obtaining the polarization current, we consider a one-dimensional case, integrating only over $p = p_{\parallel}$, which lies along the direction of the electric field (28). The integration limits are chosen appropriately to ensure that the main contribution comes from the relevant momentum range, denoted as p_{cut}.

Figure 9 plots the polarization current $J_P(t) = (\frac{\pi}{e})J_{pol.}(t)$, numerically integrated for $E_0 = 0.2E_c$ and $\tau = 10[m^{-1}]$. $J_P(t)$ rises from zero once the electric field grows non-negligible. $J_P(t)$ shows a positive peak followed by a negative dip, capturing the vacuum polarization's response to the field. The sign change occurs due to the reversal in the field strength as $E(t)$ transitions from increasing to decreasing. After the field diminishes, the polarization current does not vanish but exhibits regular oscillation similar to the trends shown by the $u(p, t)$ in the late time region. This similar behavior is shown by the polarization pressure $P_{pol.}$, see the ref. [89] for time-dependent mass configuration. At asymptotic times ($t >> \tau$), $J_P(t)$ exhibits undamped oscillations (see insert Fig. 9).

In the plot 10 shows the temporal evolution of the polarization current $J_P(t)$ for different field strengths. The red curve ($E_0 = 0.3E_c$) has a significantly larger peak and overall magnitude compared to the blue curve ($E_0 = 0.1$). This is expected because the polarization current is driven by the external field, and a strong field induces a larger current response. The overall shape of both curves remains similar, indicating that the polarization current follows a similar evolution regardless of field strength. However, the stronger field ($E_0 = 0.3$) leads to a sharper rise and decay, implying a more intense response in particle dynamics. Figure 11 represents the polarization current $J_P(t)$ for different pulse durations. For $\tau = 5$(blue curve), the current peaks sharply and localizes in time, with higher amplitude reflecting the rapid field variation. For $\tau = 25$ (red curve), the response broadens temporally with reduced peak amplitude The peak amplitude is lower, as the field varies more gradually. At $t >> \tau$, the current decays but retains oscillations, especially for $\tau = 5$.

6 Effect of basis dependence on the polarization current

The time-dependent particle number $\mathcal{N}(p, t)$ depends on the choice of adiabatic basis functions $\mathcal{W}(p, t)$ and $\mathcal{Y}(p, t)$. Figure 12 compares $\mathcal{N}(p, t)$ for two standard WKB-inspired choices: $\mathcal{W}(p, t) = \omega(p, t)$ with $\mathcal{Y}(p, t) = 0$ (as used in [70]), and $\mathcal{W}(p, t) = \omega(p, t)$, $\mathcal{Y}(p, t) = \dot{\omega}(p, t)/(2\omega(p, t)^2)$ [59].

For $t < 0$, $\mathcal{N}(p, t)$ grows faster for $\mathcal{Y}(p, t) = 0$ (blue) than for $\mathcal{Y}(p, t) \neq 0$ (red), indicating sensitivity to the basis choice. During the interaction period ($-10 < t < 20$), the blue curve exhibits stronger oscillations, whereas the red curve follows a smoother trend. At late times ($t > 20$), both curves stabilize and approach their asymptotic values; however, oscillations persist longer in the blue curve, while the red curve converges more smoothly. The second panel magnifies the late-time behavior ($t > 20$), highlighting these differences. The persistent oscillations in the blue curve suggest that omitting $\mathcal{Y}(p, t)$ introduces additional transient effects.

The central challenge in time-dependent pair production is to identify observables that remain well-defined at all times, not only in the asymptotic limit. In this regard, the current serves as a good candidate for such a physical observable.

To further investigate the effect of basis choice, we examine the *conduction* and *polarization* currents, which together constitute the total current $J(t)$. As discussed above, $J(t)$, defined through the expectation value of the gauge-invariant Noether current operator in the in-vacuum, represents a measurable quantity. In principle, the sum of the conduction and polarization components also carries physical significance. We therefore analyze how the choice of basis influences the two components of the total induced current, $J_{\text{cond}}(t)$ and $J_{\text{pol}}(t)$.

We begin with the conduction current, defined as:

$$J_{\text{cond}}(t) \propto \int dp \, \frac{p - eA(t)}{\omega(p, t)} \mathcal{N}(p, t).$$

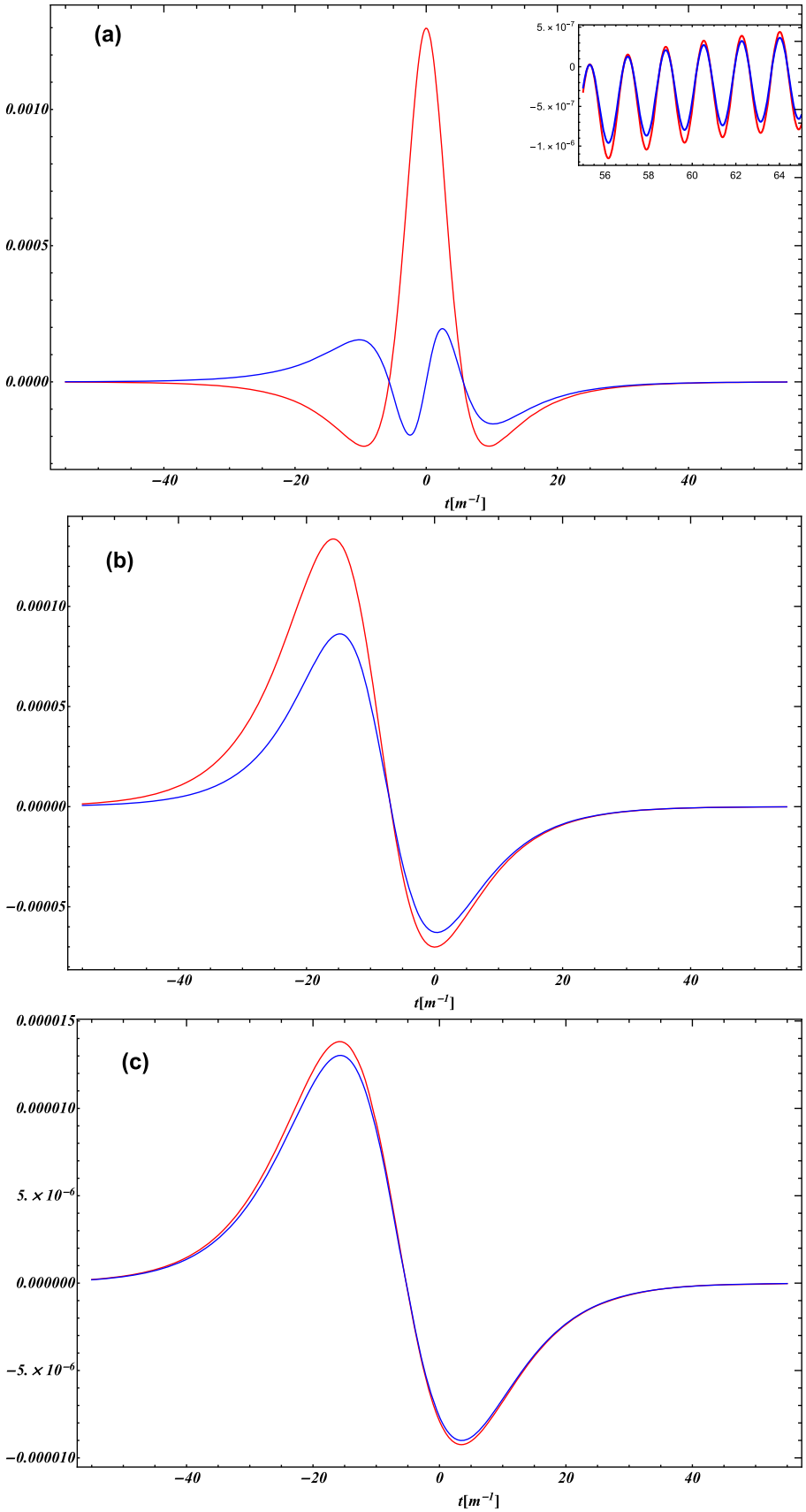

Fig. 7 The integrated $J_{pol}(t)$ in (52) with blue curve and $u(p, t)$ (red curve) with different momentum values, (a) p =0, (b) p =2, (c) p=4. All the units are taken in electron mass unit. The field parameters are $E_0 = 0.1E_c$ and $\tau = 15[m^{-1}]$

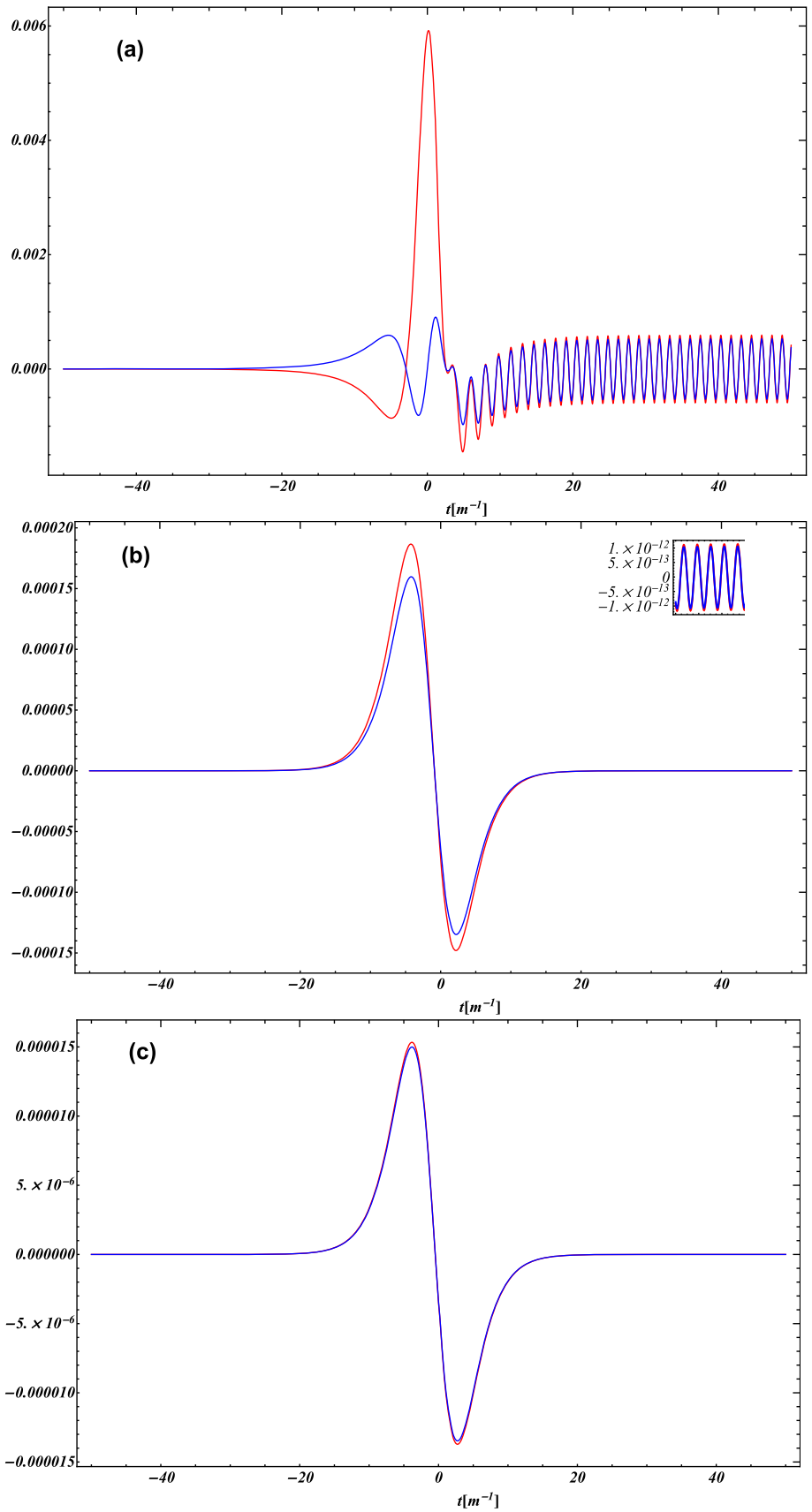

Fig. 8 The integrated $J_{pol}(t)$ in (52) with blue curve and, $u(p, t)$ (red curve) with different momentum values, (a) p =0, (b) p =2, (c) p=4. The field parameters are $E_0 = 0.1E_c$ and $\tau = 5[m^{-1}]$

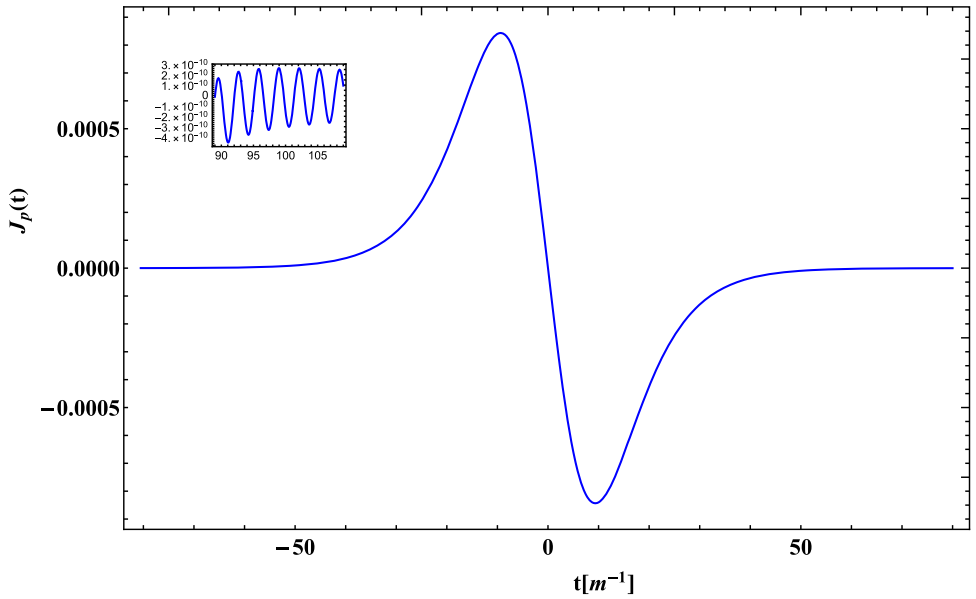

Fig. 9 Temporal dependence of polarization current $J_{pol}(t)$ defined in (52) for field parameter $E_0 = 0.2E_c$ with $\tau = 10[m^{-1}]$

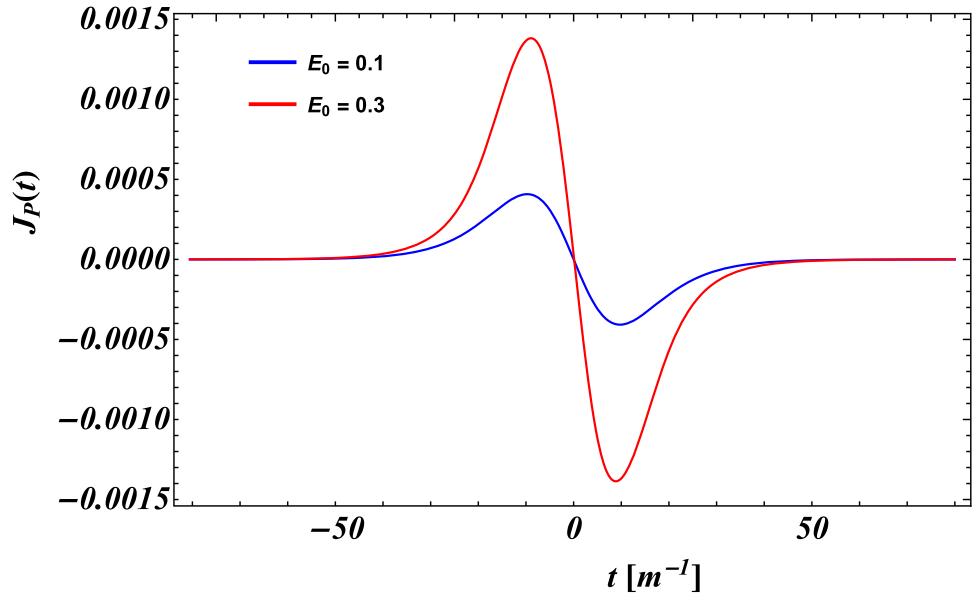

Fig. 10 Temporal dependence of polarization current $J_{pol}(t)$ defined in (52) for different field strength $E_0 = 0.1$(blue), 0.3(red) with $\tau = 15[m^{-1}]$

Since $\mathcal{N}(p, t)$ is highly basis-dependent (Fig. 12), it follows directly that $J_{\text{cond}}(t)$ must also inherit this dependence. This is confirmed numerically in Fig. 15, where the conduction current calculated in the two different bases shows substantial discrepancies in both amplitude and phase during the main interaction period. This confirms that the conduction current, which represents the transport of real particles, lacks a unique physical definition while the external field is active.

Let us now contrast this with the polarization current and its underlying function. The polarization current is defined as:

$$J_{\text{pol}}(t) \propto \int dp \, \frac{p - eA(t)}{\omega(p, t)} \, u(p, t),$$

where $u(p, t) = \text{Re}[\mathcal{C}(p, t)]$. First, it is instructive to examine the basis dependence of $u(p, t)$ itself. Figure 13 shows the evolution of $u(p, t)$ for the two different adiabatic bases. While the curves are very similar, minor differences are observable, particularly in the amplitude and precise shape of the transient peak. This indicates that $u(p, t)$, being part of the Bogoliubov coefficient structure, is not completely immune to the basis choice. However, the finding of our work is that the physically meaningful quantity polarization current $J_{pol}(t)$ is unaffected by the choice of adiabatic basis. This is demonstrated in Fig. 14, which shows that $J_{pol}(t)$ is identical for both bases. The resolution to this apparent contradiction—where $u(p, t)$ shows slight basis dependence but $J_P(t)$ does not—lies in the relationship between the total current and its components. The total induced current $J(t) = J_{\text{cond}}(t) + J_{\text{pol}}(t)$ is a basis-independent observable, as it is derived from the renormalized Noether current. During the main interaction period $(-2\tau < t < 2\tau)$,

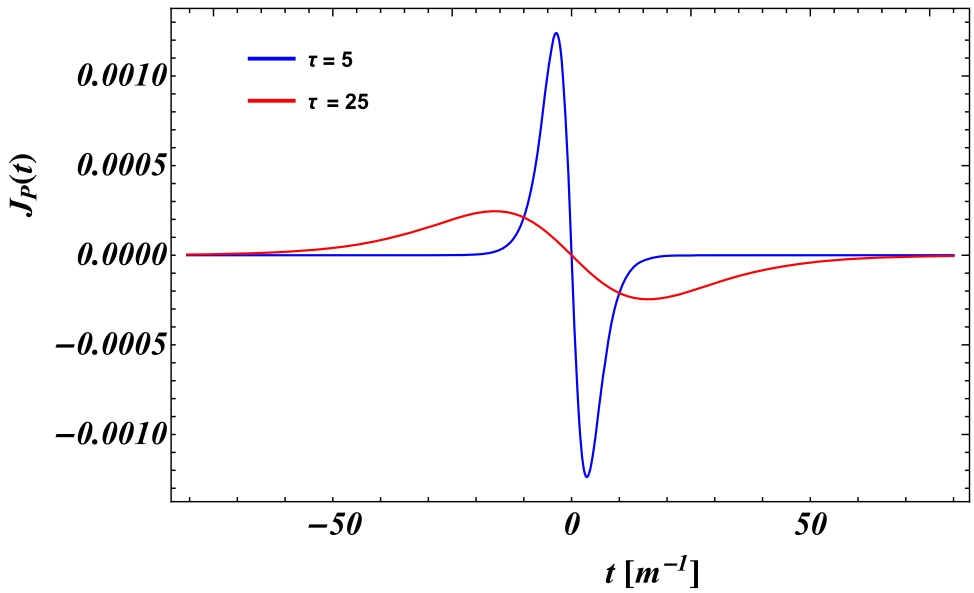

Fig. 11 Temporal dependence of polarization current $J_{pol}(t)$ defined in (52) for different pulse length $\tau = 5$(blue), 25(red) with $E_0 = 0.1E_c$

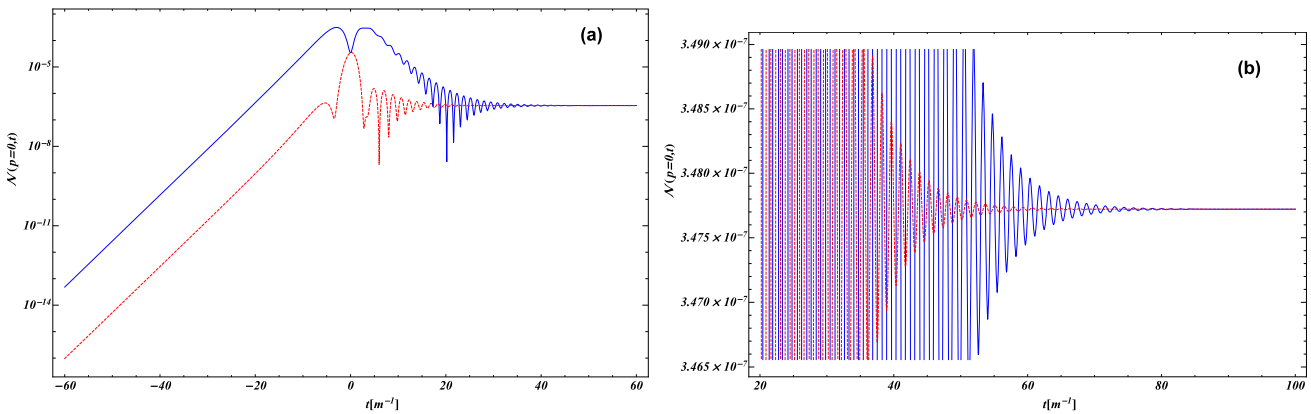

Fig. 12 Evolution of $\mathcal{N}(p,\ t)$ for two basis choices. The blue curve represents first choice of adiabatic frequency $\mathcal{W}(p,\ t) = \omega(p,\ t)$ and $\mathcal{Y}(p,\ t) = 0$ and dashed red curve for second choice $\mathcal{W}(p,\ t) = \omega(p,\ t)$ and $\mathcal{Y}(p,\ t) = \frac{\dot{\omega}(p,t)}{2\omega(p,t)^2}$. The field parameters are $E_0 = 0.2E_c$ and $\tau = 10[m^{-1}]$. The momentum is considered to be zero, and all the units are taken in the electron mass unit

the conduction current $J_{\text{cond}}(t)$ is small because the population of real particles is low. Consequently, the total current is dominated by the polarization component:

$$J(t) \approx J_{\text{pol}}(t).$$

Therefore, since $J(t)$ is basis-independent and $J(t) \approx J_{\text{pol}}(t)$, the polarization current $J_{\text{pol}}(t)$ itself must also be basis-independent. The minor basis-dependent variations in the local function $u(p,\ t)$ are precisely compensated for during the momentum integration, and potentially by counter-balancing variations in the conduction current, to yield a physical observable $J_P(t)$. This conclusion is powerfully confirmed by the numerical evidence. Unlike $\mathcal{N}(p,\ t)$ and $J_{\text{cond}}(t)$, which vary significantly with the adiabatic basis (Figs. 12, 15), $J_P(t)$ is fundamentally unaffected by this choice (Fig. 14), thus preserving its physical meaning throughout the evolution.

The physical reality of the polarization current is further supported by experimental analogs. In Dirac materials like graphene, experiments measuring nonlinear current–voltage responses attribute these signals to electron–hole pair creation [25, 30, 31, 90]. The measured current in these experiments corresponds directly to the induced polarization current described here, providing strong empirical evidence for its measurability.The polarization current can emerge as the definitive observable for studying strong-field pair production. The total induced current $J(t)$ is a gauge-invariant, basis-independent quantity. During the pair-creation process, $J(t)$ is dominated by $J_{\text{pol}}(t)$. Numerical evidence confirms that $J_{\text{pol}}(t)$ is unaffected under changes of the adiabatic basis. Experimental analogs in condensed matter systems confirm its physical reality [30, 91].

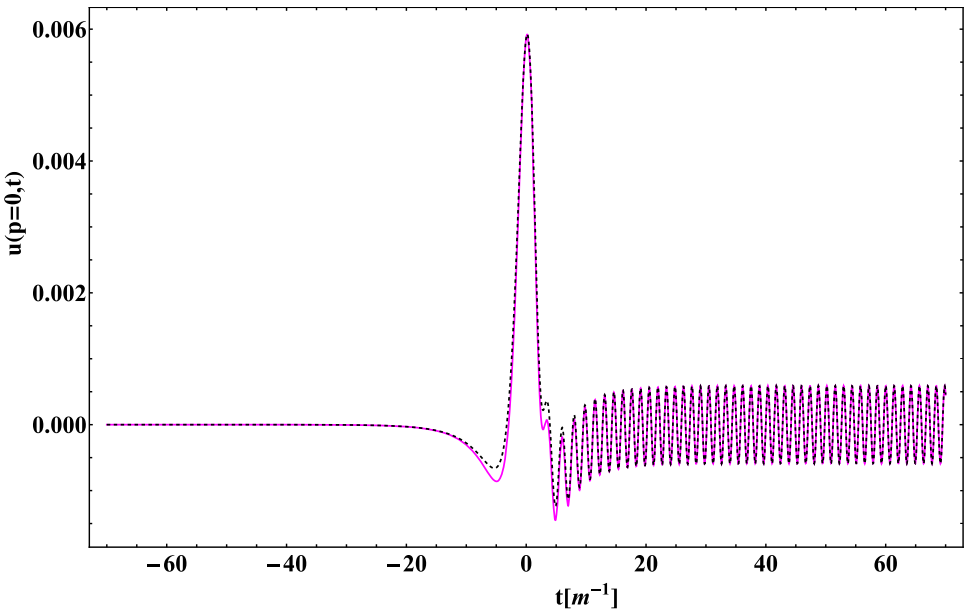

Fig. 13 Evolution of $u(p, t)$ for two basis choices. The magenta curve represent first choice of adiabatic frequency $\mathcal{W}(p, t) = \omega(p, t)$ and $\mathcal{Y}(p, t) = 0$ and dashed black curve for second choice $\mathcal{W}(p, t) = \omega(p, t)$ and $\mathcal{Y}(p, t) = \frac{\dot{\omega}(p,t)}{2\omega(p,t)^2}$. The field parameters are $E_0 = 0.2E_c$ and $\tau = 10[m^{-1}]$. The momentum is considered to be zero, and all the units are taken in the electron mass unit

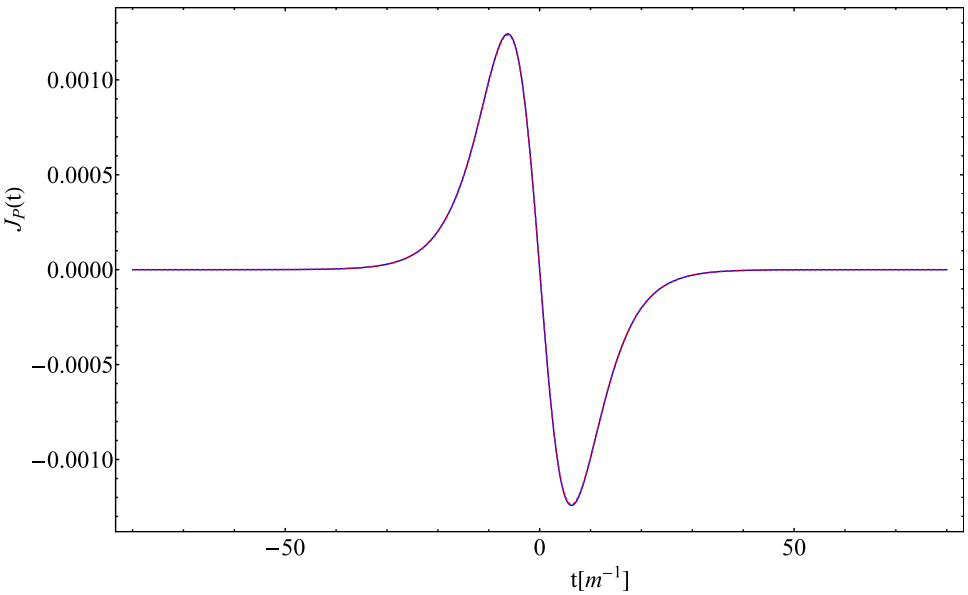

Fig. 14 Time evolution of the polarization current $J_P(t)$ evaluated in two different adiabatic bases. The blue curve corresponds to the first choice, $\mathcal{W}(p, t) = \omega(p, t)$, $\mathcal{Y}(p, t) = 0$; the dashed red curve corresponds to the second choice, $\mathcal{W}(p, t) = \omega(p, t)$, $\mathcal{Y}(p, t) = \dot{\omega}(p, t)/(2\omega(p, t)^2)$. The field parameters are $E_0 = 0.2\ E_c$ and $\tau = 10[m^{-1}]$

7 Conclusion

We investigated vacuum pair production under a time-dependent Sauter pulse $E(t) = E_0\ \mathrm{sech}^2(t/\tau)$ via canonical quantization of scalar QED. We derived generalized expressions for $\mathcal{N}(p, t)$ and $\mathcal{C}(p, t)$ through Bogoliubov transformations accommodating arbitrary adiabatic bases. Our analysis quantified how field strength E_0 and pulse duration τ governs the evolution of the particle number and vacuum polarization effects encoded in $u(p, t)$ and $v(p, t)$. The correlation function's real part $u(p, t)$ encodes vacuum polarization, while its imaginary part $v(p, t)$ corresponds to the depolarization counter-term, where computed using exact mode function solutions. We found that both functions remain negligible at early times, exhibit a strong transient peak at $t = 0$, and display oscillatory behavior at late times. Crucially,$v(p, t)$ exhibits antisymmetry about $t = 0$, whereas $u(p, t)$ shows symmetric peaks, revealing the competition between polarization and depolarization. The field strength E_0 significantly impacts the magnitude and frequency of oscillations, with stronger fields leading to more pronounced responses. Additionally, the pulse duration τ modulates the peak values and the persistence of oscillations, revealing the temporal characteristics of vacuum fluctuations. At asymptotic times, the oscillations stabilize, marking a transition to a final equilibrium state where real particle formation dominates. We also investigated the dynamical properties of the vacuum polarization current $J_P(t)$, which depends on the rate of particle creation and is directly related to the vacuum polarization function $u(p, t)$. The integrand of $J_P(t)$ exhibits a peak around the field maximum, followed by oscillatory behavior. A shorter pulse results in stronger oscillations and a broader frequency response, whereas longer

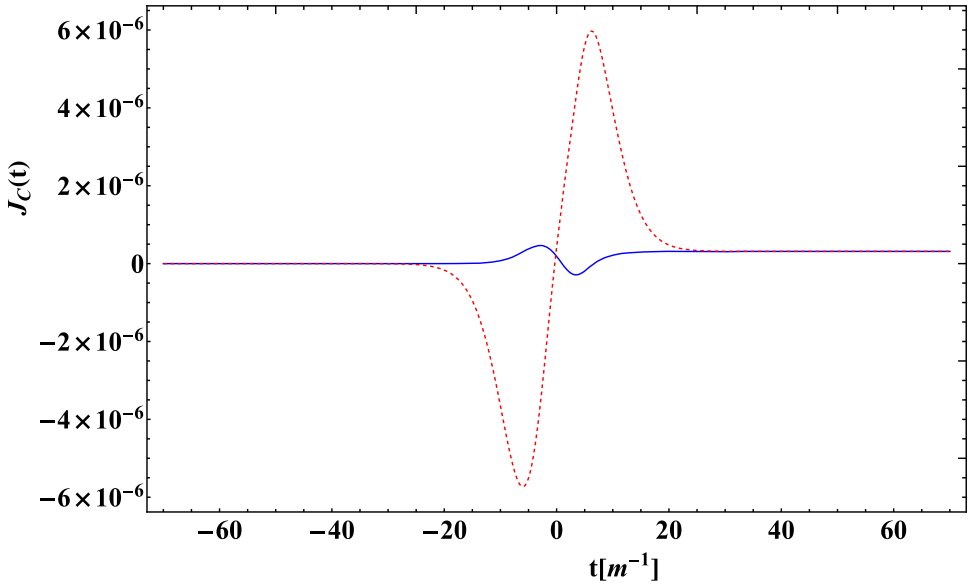

Fig. 15 The time evolution of the conduction current, $J_C(t) = (\frac{\pi}{e})J_{cond}(t)$, defined with respect to two different adiabatic bases. The blue curve represents the first choice of adiabatic frequency $\mathcal{W}(p, t) = \omega(p, t)$ and $\mathcal{Y}(p, t) = 0$ and dashed red curve for the second choice $\mathcal{W}(p, t) = \omega(p, t)$ and $\mathcal{Y}(p, t) = \frac{\dot{\omega}(p,t)}{2\omega(p,t)^2}$. The field parameters are $E_0 = 0.2E_c$ and $\tau = 10[m^{-1}]$

pulses lead to smoother variations. The field strength determines the peak magnitude and oscillation characteristics, with higher values inducing sharper transitions.

Furthermore, we examined the dependence of the time-dependent particle number $\mathcal{N}(p, t)$ on the choice of adiabatic basis functions. Our results show that $\mathcal{N}(p, t)$ varies significantly at intermediate times depending on the basis choice, whereas the polarization current $J_{pol}(t)$ remains unaffected. Our findings demonstrate that the vacuum polarization current $J_{pol}(t)$ provides a unique and well-defined observable for tracking pair-production dynamics. Its robustness against the choice of adiabatic basis is not merely a numerical coincidence but is fundamentally guaranteed because it constitutes the dominant part of the physical, total electric current $J(t)$ at intermediate times, before the conduction current from real particles becomes significant. Overall, our findings provide deeper insight into vacuum polarization effects and the interplay between particle creation and annihilation in strong-field QED. The results emphasize the importance of polarization current as a stable observable in describing the dynamics of pair production processes.

Acknowledgements Deepak Sah acknowledges the financial assistance provided by the Raja Ramanna Center for Advanced Technology (RRCAT) and the Homi Bhabha National Institute (HBNI) for carrying out this research work.

Funding Open access funding provided by Department of Atomic Energy.

Data availability Data sharing not applicable to this article as no datasets were generated or analysed during the current study.

References

1. O. Klein, Zeitschrift Für Physik a Hadrons and Nuclei. **41**, 407–442 (1927). https://doi.org/10.1007/BF01400205
2. O. Klein, Z. Phys. **53**, 157 (1929)
3. F. Sauter, Z. Phys. **69**, 742–764 (1931)
4. F. Sauter, Z. Phys. **73**, 547–552 (1932). https://doi.org/10.1007/BF01349862
5. L. Parker, Phys. Rev. **183**, 1057–1068 (1969). https://doi.org/10.1103/PhysRev.183.1057
6. G.W. Gibbons, S.W. Hawking, Phys. Rev. D **15**, 2738–2751 (1977). https://doi.org/10.1103/PhysRevD.15.2738
7. W. Heisenberg, H. Euler, Z. Phys. **98**, 714–732 (1936)
8. J.S. Schwinger, Phys. Rev. **82**, 664–679 (1951). https://doi.org/10.1103/PhysRev.82.664
9. J. Schwinger, Dover Publications, 1958, ISBN 978-0-486-60444-2, 978-0-486-60444-2
10. ELI, https://eli-laser.eu/
11. T. Heinzl, A. Ilderton, Eur. Phys. J. D **55**, 359–364 (2009). https://doi.org/10.1140/epjd/e2009-00113-x. [arXiv:0811.1960 [hep-ph]]
12. G.V. Dunne, Eur. Phys. J. D **55**, 327–340 (2009). https://doi.org/10.1140/epjd/e2009-00022-0. [arXiv:0812.3163 [hep-th]]
13. Deutsches Elektronen-Synchrotron DESY, http://www.desy.de/
14. A. Ringwald, Phys. Lett. B **510**, 107–116 (2001). https://doi.org/10.1016/S0370-2693(01)00496-8. [arXiv:hep-ph/0103185 [hep-ph]]

15. CoReLS, http://corels.ibs.re.kr/
16. J. Andruszkow et al., Phys. Rev. Lett. **85**, 3825–3829 (2000). https://doi.org/10.1103/PhysRevLett.85.3825. [arXiv:physics/0006010 [physics]]
17. D.L. Burke, R.C. Field, G. Horton-Smith, T. Kotseroglou, J.E. Spencer, D. Walz, S.C. Berridge, W.M. Bugg, K. Shmakov, A.W. Weidemann et al., Phys. Rev. Lett. **79**, 1626–1629 (1997). https://doi.org/10.1103/PhysRevLett.79.1626
18. T. Yu, F. Pegoraro, G. Sarri, D.A. Reis, Eur. Phys. J. D. **77**, 55 (2023)
19. A. Fedotov, A. Ilderton, F. Karbstein, B. King, D. Seipt, H. Taya, G. Torgrimsson, Phys. Rept. **1010**, 1–138 (2023). https://doi.org/10.1016/j.physrep.2023.01.003. [arXiv:2203.00019 [hep-ph]]
20. A. Schmitt, P. Vallet, D. Mele, M. Rosticher, T. Taniguchi, K. Watanabe, E. Bocquillon, G. Fève, J.M. Berroir, C. Voisin et al., Nature Phys. **19**(6), 830–835 (2023). https://doi.org/10.1038/s41567-023-01978-9. [arXiv:2207.13400 [cond-mat.mes-hall]]
21. S. Villalba-Chávez, O. Mathiak, R. Egger, C. Müller, Phys. Rev. D **108**(11), 116007 (2023). https://doi.org/10.1103/PhysRevD.108.116007. [arXiv:2211.04206 [cond-mat.mes-hall]]
22. A.H. Castro Neto, F. Guinea, N.M.R. Peres, K.S. Novoselov, A.K. Geim, Rev. Mod. Phys. **81**, 109–162 (2009). https://doi.org/10.1103/RevModPhys.81.109. [arXiv:0709.1163 [cond-mat.other]]
23. M.A.H. Vozmediano, M.I. Katsnelson, F. Guinea, Phys. Rept. **496**, 109–148 (2010). https://doi.org/10.1016/j.physrep.2010.07.003. [arXiv:1003.5179 [cond-mat.mes-hall]]
24. D. Allor, T.D. Cohen, D.A. McGady, Phys. Rev. D **78**, 096009 (2008). https://doi.org/10.1103/PhysRevD.78.096009. [arXiv:0708.1471 [cond-mat.mes-hall]]
25. S.A. Smolyansky, A.D. Panferov, D.B. Blaschke, N.T. Gevorgyan, Particles **2**(2), 208–230 (2019). https://doi.org/10.3390/particles2020015
26. G.L. Klimchitskaya, V.M. Mostepanenko, Phys. Rev. D **87**(12), 125011 (2013). https://doi.org/10.1103/PhysRevD.87.125011. [arXiv:1305.5700 [hep-th]]
27. G.W. Semenoff, Phys. Rev. Lett. **53**, 2449 (1984). https://doi.org/10.1103/PhysRevLett.53.2449
28. M. Lewkowicz, H. Kao, B. Rosenstein, B. Rosenstein, B. Rosenstein, Phys. Rev. B. **84**, 035414 (2011). https://api.semanticscholar.org/CorpusID:119235201
29. N. Vandecasteele, A. Barreiro, M. Lazzeri, A. Bachtold, F. Mauri, Phys. Rev. B. **82**, 045416 (2010). https://doi.org/10.1103/PhysRevB.82.045416
30. S.A. Smolyansky, D.V. Churochkin, V.V. Dmitriev, A.D. Panferov, B. Kämpfer, EPJ Web Conf. **138**, 06004 (2017). https://doi.org/10.1051/epjconf/201713806004
31. S.A. Smolyansky, A.D. Panferov, D.B. Blaschke, N.T. Gevorgyan, Particles **3**(2), 456–476 (2020). https://doi.org/10.3390/particles3020032. [arXiv:2004.03759 [physics.optics]]
32. A. Panferov, S. Smolyansky, D. Blaschke, N. Gevorgyan, EPJ Web Conf. **204**, 06008 (2019). https://doi.org/10.1051/epjconf/201920406008. [arXiv:1901.01395 [cond-mat.mes-hall]]
33. V. Yakimenko, S. Meuren, F. Del Gaudio, C. Baumann, A. Fedotov, F. Fiuza, T. Grismayer, M.J. Hogan, A. Pukhov, L.O. Silva et al., Phys. Rev. Lett. **122**(19), 190404 (2019). https://doi.org/10.1103/PhysRevLett.122.190404. [arXiv:1807.09271 [physics.plasm-ph]]
34. A. Di Piazza, C. Muller, K.Z. Hatsagortsyan, C.H. Keitel, Rev. Mod. Phys. **84**, 1177 (2012). https://doi.org/10.1103/RevModPhys.84.1177. [arXiv:1111.3886 [hep-ph]]
35. L.H. Ford, Rept. Prog. Phys. **84**(11), 116901 (2021). https://doi.org/10.1088/1361-6633/ac1b23. [arXiv:2112.02444 [gr-qc]]
36. Á. Álvarez-Domínguez, J.A.R. Cembranos, L.J. Garay, M. Martín-Benito, Á. Parra-López, J.M. Sánchez Velázquez, Phys. Rev. D **108**(6), 065008 (2023). https://doi.org/10.1103/PhysRevD.108.065008. [arXiv:2303.07436 [hep-th]]
37. A. Blinne, H. Gies, F. Karbstein, C. Kohlfürst, M. Zepf, Phys. Rev. D **99**(1), 016006 (2019). https://doi.org/10.1103/PhysRevD.99.016006. [arXiv:1811.08895 [physics.optics]]
38. J. Cortez, G.A.M. Marugán, J. Velhinho, Mathematics **8**(1), 115 (2020). https://doi.org/10.3390/math8010115. [arXiv:1912.04203 [gr-qc]]
39. J. Cortez, G.A.M. Marugán, J.M. Velhinho, Universe **7**(8), 299 (2021). https://doi.org/10.3390/universe7080299. [arXiv:2108.07489 [gr-qc]]
40. C. Lueders, J.E. Roberts, Commun. Math. Phys. **134**, 29–63 (1990). https://doi.org/10.1007/BF02102088
41. B. Elizaga Navascués, G.A.M. Marugán, T. Thiemann, Quant. Grav. **36**(18), 185010 (2019). https://doi.org/10.1088/1361-6382/ab32af. [arXiv:1903.05695 [gr-qc]]
42. M.J. Fahn, K. Giesel, M. Kobler, Universe **5**(7), 170 (2019). https://doi.org/10.3390/universe5070170. [arXiv:1812.11122 [gr-qc]]
43. I. Agullo, W. Nelson, A. Ashtekar, Phys. Rev. D **91**, 064051 (2015). https://doi.org/10.1103/PhysRevD.91.064051. [arXiv:1412.3524 [gr-qc]]
44. Y. Yamada, JCAP **09**, 009 (2021). https://doi.org/10.1088/1475-7516/2021/09/009. [arXiv:2106.06111 [hep-th]]
45. R. Dabrowski, G.V. Dunne, Phys. Rev. D **90**(2), 025021 (2014). https://doi.org/10.1103/PhysRevD.90.025021. [arXiv:1405.0302 [hep-th]]
46. H. Taya, T. Fujimori, T. Misumi, M. Nitta, N. Sakai, JHEP **03**, 082 (2021). https://doi.org/10.1007/JHEP03(2021)082. [arXiv:2010.16080 [hep-th]]
47. R. Dabrowski, G.V. Dunne, Phys. Rev. D **94**(6), 065005 (2016). https://doi.org/10.1103/PhysRevD.94.065005. [arXiv:1606.00902 [hep-th]]
48. D.B. Blaschke, B. Kämpfer, S.M. Schmidt, A.D. Panferov, A.V. Prozorkevich, S.A. Smolyansky, Phys. Rev. D **88**(4), 045017 (2013). https://doi.org/10.1103/PhysRevD.88.045017. [arXiv:1301.1640 [physics.plasm-ph]]
49. G. Gregori, D.B. Blaschke, P.P. Rajeev, H. Chen, R.J. Clarke, T. Huffman, C.D. Murphy, A.V. Prozorkevich, C.D. Roberts, G. Ropke et al., High Energy Dens. Phys. **6**, 166 (2010). https://doi.org/10.1016/j.hedp.2009.11.001. [arXiv:1005.3280 [hep-ph]]
50. N.B. Narozhnyi, A.I. Nikishov, Yad. Fiz. **11**, 1072 (1970)
51. S.P. Gavrilov, D.M. Gitman, Phys. Rev. D **53**, 7162–7175 (1996). https://doi.org/10.1103/PhysRevD.53.7162. [arXiv:hep-th/9603152 [hep-th]]
52. F. Hebenstreit, R. Alkofer, H. Gies, Phys. Rev. D **82**, 105026 (2010). https://doi.org/10.1103/PhysRevD.82.105026. [arXiv:1007.1099 [hep-ph]]
53. C. Banerjee, M.P. Singh, Phys. Rev. D **105**(7), 076021 (2022). https://doi.org/10.1103/PhysRevD.105.076021. [arXiv:1807.06951 [physics.plasm-ph]]
54. F. Gelis, N. Tanji, Prog. Part. Nucl. Phys. **87**, 1–49 (2016). https://doi.org/10.1016/j.ppnp.2015.11.001. [arXiv:1510.05451 [hep-ph]]
55. D. Sah, M.P. Singh, Acta Phys. Polon. A **148**(2), 149 (2025). https://doi.org/10.12693/aphyspola.148.149
56. D.B. Blaschke, A.V. Prozorkevich, G. Ropke, C.D. Roberts, S.M. Schmidt, D.S. Shkirmanov, S.A. Smolyansky, Eur. Phys. J. D **55**, 341–358 (2009). https://doi.org/10.1140/epjd/e2009-00156-y. [arXiv:0811.3570 [physics.plasm-ph]]
57. S.A. Smolyansky, A.D. Panferov, D.B. Blaschke, L. Juchnowski, B. Kämpfer, A. Otto, Russ. Phys. J. **59**(11), 1731–1738 (2017). https://doi.org/10.1007/s11182-017-0970-5. [arXiv:1607.08775 [hep-ph]]
58. A.M. Fedotov, E.G. Gelfer, K.Y. Korolev, S.A. Smolyansky, Phys. Rev. D **83**, 025011 (2011). https://doi.org/10.1103/PhysRevD.83.025011. [arXiv:1008.2098 [hep-ph]]
59. S.M. Schmidt, D. Blaschke, G. Ropke, S.A. Smolyansky, A.V. Prozorkevich, V.D. Toneev, Int. J. Mod. Phys. E **7**, 709–722 (1998). https://doi.org/10.1142/S0218301398000403. [arXiv:hep-ph/9809227 [hep-ph]]
60. Y. Kluger, J.M. Eisenberg, B. Svetitsky, F. Cooper, E. Mottola, Phys. Rev. D **45**, 4659–4671 (1992). https://doi.org/10.1103/PhysRevD.45.4659
61. Y. Kluger, E. Mottola, J.M. Eisenberg, Phys. Rev. D **58**, 125015 (1998). https://doi.org/10.1103/PhysRevD.58.125015. [arXiv:hep-ph/9803372 [hep-ph]]
62. A.A. Grib, V.M. Mostepanenko, V.M. Frolov, Teor. Mat. Fiz. **13**, 377–390 (1972). https://doi.org/10.1007/BF01036146

63. S. Habib, C. Molina-Paris, E. Mottola, Phys. Rev. D **61**, 024010 (2000). https://doi.org/10.1103/PhysRevD.61.024010. [arXiv:gr-qc/9906120 [gr-qc]]
64. L.J. Garay, A. García Martín-Caro, M. Martín-Benito, JHEP **04**, 120 (2020). https://doi.org/10.1007/JHEP04(2020)120. [arXiv:1911.03205 [hep-th]]
65. S. Winitzki, Phys. Rev. D **72**, 104011 (2005). https://doi.org/10.1103/PhysRevD.72.104011. [arXiv:gr-qc/0510001 [gr-qc]]
66. S. Enomoto, T. Matsuda, JHEP **03**, 090 (2021). https://doi.org/10.1007/JHEP03(2021)090. [arXiv:2010.14835 [hep-ph]]
67. C.K. Dumlu, G.V. Dunne, Phys. Rev. Lett. **104**, 250402 (2010). https://doi.org/10.1103/PhysRevLett.104.250402. [arXiv:1004.2509 [hep-th]]
68. S. Hashiba, S. Ling, A.J. Long, JHEP **09**, 216 (2022). https://doi.org/10.1007/JHEP09(2022)216. [arXiv:2206.14204 [hep-th]]
69. M.V. Barry, Proc. Roy. Soc. Lond. A **422**, 7–21 (1989). https://doi.org/10.1098/rspa.1989.0018
70. N.D. Birrell, P.C.W. Davies, *Quantum Fields in Curved Space, Cambridge Monographs on Mathematical Physics* (Cambridge University Press, Cambridge, England, 1982)
71. S. A. Smolyansky, G. Ropke, S. M. Schmidt, D. Blaschke, V. D. Toneev, A. V. Prozorkevich, [arXiv:hep-ph/9712377 [hep-ph]]
72. Y. Kluger, J.M. Eisenberg, B. Svetitsky, F. Cooper, E. Mottola, Phys. Rev. Lett. **67**, 2427–2430 (1991). https://doi.org/10.1103/PhysRevLett.67.2427
73. A. Ilderton, Phys. Rev. D **105**(1), 016021 (2022). https://doi.org/10.1103/PhysRevD.105.016021. [arXiv:2108.13885 [hep-ph]]
74. D. B. Blaschke, S. A. Smolyansky, A. Panferov, L. Juchnowski, https://doi.org/10.3204/DESY-PROC-2016-04/Blaschke[arXiv:1704.04147 [hep-ph]]
75. D.B. Blaschke, A.V. Prozorkevich, C.D. Roberts, S.M. Schmidt, S.A. Smolyansky, Phys. Rev. Lett. **96**, 140402 (2006). https://doi.org/10.1103/PhysRevLett.96.140402. [arXiv:nucl-th/0511085 [nucl-th]]
76. N. Ahmadiniaz, S.P. Kim, C. Schubert, J. Phys. Conf. Ser. **2249**(5), 012020 (2022). https://doi.org/10.1088/1742-6596/2249/1/012020. [arXiv:2205.15945 [hep-th]]
77. D. Sah, M. P. Singh, [arXiv:2309.12079 [hep-ph]]
78. C. Muller, K.Z. Hatsagortsyan, C.H. Keitel, Phys. Lett. B **659**, 209–213 (2008). https://doi.org/10.1016/j.physletb.2007.11.002. [arXiv:0705.0917 [hep-ph]]
79. M. Abramowitz, , I. Stegun, Handbook of Mathematical Functions with Formulas, Graphs, and Mathematical Tables. (Dover,1964)
80. C. Banerjee, M.P. Singh, Phys. Rev. D **100**(5), 056016 (2019). https://doi.org/10.1103/PhysRevD.100.056016. [arXiv:1809.06901 [hep-ph]]
81. I.A. Aleksandrov, V.V. Dmitriev, D.G. Sevostyanov, S.A. Smolyansky, Eur. Phys. J. ST **229**(22–23), 3469–3485 (2020). https://doi.org/10.1140/epjst/e2020-000056-1. [arXiv:2004.02179 [hep-ph]]
82. M. D. Schwartz, Cambridge University Press, (2014), ISBN 978-1-107-03473-0, 978-1-107-03473-0
83. M. Peskin, D. Schroeder, *An Introduction to Quantum Field Theory* (Westview Press, Cambridge, 1995)
84. H. Al-Naseri, G. Brodin, Phys. Rev. E **108**(5), 055205 (2023). https://doi.org/10.1103/PhysRevE.108.055205. [arXiv:2305.10106 [physics.plasm-ph]]
85. J.F. Dawson, B. Mihaila, F. Cooper, Phys. Rev. D **80**, 014011 (2009). https://doi.org/10.1103/PhysRevD.80.014011. [arXiv:0906.2225 [hep-ph]]
86. B. Dóra, R. Moessner, Phys. Rev. B. **81**, 165431 (2010). https://doi.org/10.1103/PhysRevB.81.165431
87. D.V. Vinnik, A.V. Prozorkevich, S.A. Smolyansky, V.D. Toneev, M.B. Hecht, C.D. Roberts, S.M. Schmidt, Eur. Phys. J. C **22**, 341–349 (2001). https://doi.org/10.1007/s100520100787. [arXiv:nucl-th/0103073 [nucl-th]]
88. A. Ferreiro, J. Navarro-Salas, S. Pla, Phys. Rev. D **98**(4), 045015 (2018). https://doi.org/10.1103/PhysRevD.98.045015. [arXiv:1807.10361 [gr-qc]]
89. A.V. Filatov, A.V. Prozorkevich, S.A. Smolyansky, V.D. Toneev, Phys. Part. Nucl. **39**, 886–911 (2008). https://doi.org/10.1134/S1063779608060026. [arXiv:0710.0233 [hep-ph]]
90. S.P. Gavrilov, D.M. Gitman, N. Yokomizo, Phys. Rev. D **86**, 125022 (2012). https://doi.org/10.1103/PhysRevD.86.125022. [arXiv:1207.1749 [hep-th]]
91. H.C. Kao, M. Lewkowicz, B. Rosenstein, Phys. Rev. B **82**, 035406 (2010). https://doi.org/10.1103/PhysRevB.82.035406. [arXiv:1004.1144 [cond-mat.mes-hall]]